



CHORUS

This is the accepted manuscript made available via CHORUS. The article has been published as:

## Amplitude equations for reaction-diffusion systems with cross diffusion

Evgeny P. Zemskov, Vladimir K. Vanag, and Irving R. Epstein

Phys. Rev. E **84**, 036216 — Published 26 September 2011

DOI: [10.1103/PhysRevE.84.036216](https://doi.org/10.1103/PhysRevE.84.036216)

# **Amplitude equations for reaction-diffusion systems with cross-diffusion**

Evgeny P. Zemskov, Vladimir K. Vanag and Irving R. Epstein\*

*Department of Chemistry, MS 015, Brandeis University, Waltham, 02454-9110 USA.*

*Abstract.* Using Taylor series expansion, multi-scaling, and further expansion in powers of a small parameter, we develop general amplitude equations for two-variable reaction-diffusion systems with cross-diffusion terms in the cases of Hopf and Turing instabilities. We apply this analysis to the Oregonator and Brusselator models and find that inhibitor cross-diffusion induced by the activator and activator cross-diffusion induced by the inhibitor have opposite effects in the two models as a result of the different structure of their community matrices. Our analysis facilitates finding regions of supercritical and subcritical bifurcations, as well as wave- and anti-wave domains and domains of turbulent waves in the case of Hopf instability.

\* Author to whom correspondence should be addressed. Email: [epstein@brandeis.edu](mailto:epstein@brandeis.edu).

## 1. Introduction

The effects of cross-diffusion, the phenomenon in which a gradient in the concentration of one species induces fluxes of other species, on pattern formation in reaction-diffusion systems have been discussed in many theoretical papers (for a review see Ref. [1]). In general, cross-diffusion can modify any type of pattern, stationary, periodic or chaotic, and can even induce diffusive instability, Turing or wave [2,3]. Recent experiments [4-6] on the Belousov-Zhabotinsky reaction in a reverse microemulsion (BZ-AOT system [7]) have revealed that significant cross-diffusion takes place in this system, and model calculations [5] suggest that cross-diffusion effects should be large enough to affect BZ-AOT patterns.

Until now, however, there has been no general analysis of the possible role of cross-diffusion in dissipative pattern formation. Such an evaluation can be obtained on the basis of amplitude equations, which provide a mathematical description of reaction-diffusion systems close to the onset of instability [8-10]. In the case of Hopf instability, responsible for the onset of homogeneous oscillations, the corresponding amplitude equation is called the complex Ginzburg-Landau equation (CGLE) [9-11], while in the case of Turing instability, responsible for the emergence of stationary, spatially periodic patterns, the amplitude equation is simply referred to as the Turing amplitude equation (TAE) [12]. The TAE bears a strong resemblance to the real version of the Ginzburg-Landau equation.

The method [9,13] of derivation of amplitude equations for reaction-diffusion systems (Kuramoto's approach) is based on multiple time and space scales, expansion of

the original nonlinear equations in Taylor series (consisting of linear, quadratic, cubic, ... operators), and further expansion of all these operators in powers of a small control parameter near the onset of instability, where the small parameter is the ratio between “small” and “large” time or space scales (as well as a measure of the deviation from the onset of instability). This approach has been used for many reaction-diffusion models, including the Brusselator [9,14], Gray-Scott, Rössler [15], FitzHugh-Nagumo [16,17], and Lengyel-Epstein models [18], as well as a model for CO oxidation on a Pt surface [19].

To date, Kuramoto’s approach has been applied only to reaction-diffusion systems with diagonal diffusion matrices. Our goal here is to extend this method to systems with cross-diffusion, where the diffusion matrix has non-zero off-diagonal elements, and apply our results to two well-known reaction-diffusion models, the Oregonator [20,21] and the Brusselator [22], which we supplement with cross-diffusion terms. For the abstract Brusselator model without cross-diffusion terms, the CGLE and TAE were deduced previously [9,12,14], whereas for the two-variable Oregonator model, despite the importance of this model in describing the well-known Belousov-Zhabotinsky reaction [23,24], there are no analytical expressions available for the coefficients of the amplitude equations. Numerical calculations were done for the CGLE coefficients of the three-variable unnormalized Oregonator model and a four-variable unnormalized Oregonator-like model [25,26]. The coefficients of the CGLE and TAE obtained in the present work for the Oregonator model, even without cross-diffusion coefficients, may have their own value, since they allow us to link experimental conditions (e.g., the concentrations of the BZ reactants) to the parameters of the amplitude equations.

The paper is organized as follows. In Section 2, we develop the mathematical procedure for the derivation of the amplitude equations in general vector form, extending Kuramoto’s approach to the cross-diffusion case. In Section 3, we specify this method to a general two-component reaction-diffusion system with cross-diffusion terms. In Section 4, we apply our general result to the Oregonator model and find the coefficients of the CGLE and the TAE. In Section 5, we present analogous results for the Brusselator model. We conclude in Section 6 with a general discussion. The equivalence of the CGLE derivation to the Kuramoto’s results is shown in [Appendix A](#). The technical details of the CGLE coefficient calculation for the Oregonator model are collected in [Appendix B](#).

## 2. General procedure

We start from a general reaction-diffusion system with cross-diffusion terms, which is described by the following equation in vector form

$$\partial \mathbf{Z} / \partial t = \mathbf{F}(\mathbf{Z}) + \mathbf{D}(\mathbf{Z}) \nabla^2 \mathbf{Z} + \nabla [\mathbf{D}(\mathbf{Z})] \nabla \mathbf{Z}, \quad (1)$$

where  $\mathbf{Z}$  is vector of variables (proportional to the concentrations of reactive species),  $\mathbf{F}(\mathbf{Z})$  is a set of reaction rate functions, and  $\mathbf{D}(\mathbf{Z})$  is a square diffusion matrix including cross-diffusion coefficients. Here we take into account that the diffusion coefficients depend in general on the concentration variables [1]. The eigenvalues of  $\mathbf{D}$  must be real and positive (this follows from the second law of thermodynamics) [1,27]. The gradient  $\nabla$  is  $\partial / \partial r$  for the one-dimensional (1D) case, where  $r$  is the spatial coordinate. If all

elements of  $\mathbf{D}$  are constants, i.e., concentration-independent, then the last term in Eq. (1) vanishes.

The dynamics of system (1) close to the Hopf instability can be described by the CGLE [9,10]

$$\partial W / \partial t = (1 + ic_0)W + (1 + ic_1)\nabla^2 W - (1 + ic_2)|W|^2 W. \quad (2)$$

The constant  $c_0$  can be eliminated by the transformation  $W \rightarrow W' \exp(ic_0 t)$ , so that Eq. (2) can be rewritten as

$$\partial W' / \partial t = W' + (1 + ic_1)\nabla^2 W' - (1 + ic_2)|W'|^2 W'. \quad (3)$$

In Eq. (2),  $W$  is the complex amplitude and the real coefficients  $c_0, c_1$  and  $c_2$  depend on the parameters of the system.

Close to the onset of Turing instability the system behavior is represented by the TAE

$$\frac{\partial W}{\partial t} = \eta W + g|W|^2 W + D_T \frac{\partial^2 W}{\partial r^2}. \quad (4)$$

Its normalized form with  $\eta = D_T = 1$  and  $g = -1$  can be considered as a limiting case of the CGLE (3) if the constants  $c_1$  and  $c_2$  are equal to zero [11]. The TAE is a valid description only in one spatial dimension (1D), the case we consider here for Turing instability. In the 2D case (which we do not consider), amplitude equations (AE) of the Newell-Whitehead-Segel type [28,29] (with more complex spatial derivatives) are often used. For this case, the number of coupled AE is equal to the number of crystallographic rotation axes (e.g., three for hexagons). In the case of hexagons, additional quadratic terms of the type  $\overline{W_i W_j}$  and new spatial terms of the form  $\overline{W_i \nabla W_j}$  emerge, where the

upper bar means complex conjugate, and indices  $i, j = 1, 2, 3$  correspond to rotation axes [30]. Application of such AE to reaction-diffusion systems can be found elsewhere [31,32]. We do not consider here the case of wave instability.

Consider now how to obtain Eqs. (2) or (4) from (1). First we linearize system (1) around the uniform steady state  $\mathbf{Z}_0$ , which satisfies the equations  $\mathbf{F}(\mathbf{Z}_0) = 0$ , introduce the deviation  $\mathbf{X} = \mathbf{Z} - \mathbf{Z}_0$  from  $\mathbf{Z}_0$ , and then express system (1) in terms of  $\mathbf{X}$  and expand it in a Taylor series:

$$\partial \mathbf{X} / \partial t = \mathbf{JX} + \mathbf{D}_0 \nabla^2 \mathbf{X} + \mathbf{MXX} + \mathbf{CXXX} + \dots, \quad (5)$$

where the Jacobian matrix  $\mathbf{J}$  has elements  $J_{ij} = \partial F_i(\mathbf{Z}) / \partial Z_j$  at  $\mathbf{Z} = \mathbf{Z}_0$  and  $\mathbf{D}_0 = \mathbf{D}(\mathbf{Z}_0)$ .

The sum of the first two terms can be considered as a linear operator,  $\mathbf{JX} + \mathbf{D}_0 \nabla^2 \mathbf{X} \equiv \mathbf{LX}$ .

The quadratic term  $\mathbf{MXX}$  consists of two parts, “chemical”  $\mathbf{HXX}$ , and “diffusive”

$\mathbf{QXX}$ :

$$\mathbf{MXX} = \mathbf{HXX} + \mathbf{QXX}, \quad (6)$$

where

$$(\mathbf{HXX})_i = \frac{1}{2!} \sum_{j,k} \left. \frac{\partial^2 F_i(\mathbf{Z})}{\partial Z_j \partial Z_k} \right|_{\mathbf{Z}=\mathbf{Z}_0} X_j X_k, \quad j, k = 1, 2, \dots \quad (7)$$

$$(\mathbf{QXX})_i = \sum_{j,k} \left. \frac{\partial D_{ij}(\mathbf{Z})}{\partial Z_k} \right|_{\mathbf{Z}=\mathbf{Z}_0} \left[ X_k \nabla^2 X_j + (\nabla X_k)(\nabla X_j) \right], \quad j, k = 1, 2, \dots \quad (8)$$

The form  $\mathbf{HXX}$  is sometimes referred to as the Hessian [25]. The cubic term  $\mathbf{CXXX}$

also consists of two parts, “chemical”  $\mathbf{NXXX}$ , and “diffusive”  $\mathbf{SXXX}$ :

$$\mathbf{CXXX} = \mathbf{NXXX} + \mathbf{SXXX}, \quad (9)$$

where

$$(NXXX)_i = \frac{1}{3!} \sum_{j,k,l} \left. \frac{\partial^3 F_i(Z)}{\partial Z_j \partial Z_k \partial Z_l} \right|_{Z=Z_0} X_j X_k X_l, \quad j,k,l=1,2,\dots \quad (10)$$

$$(SXXX)_i = \sum_{j,k,l} \left. \frac{\partial^2 D_{ij}(Z)}{\partial Z_k \partial Z_l} \right|_{Z=Z_0} \left[ \frac{1}{2} X_l X_k \nabla^2 X_j + X_l (\nabla X_k) (\nabla X_j) \right], \quad j,k,l=1,2,\dots \quad (11)$$

Next we introduce a small control parameter  $\mu$  as a normalized deviation from the critical value at which instability starts. Using this parameter, we introduce a new scaled time  $\tau$  and space  $R$  as  $\tau = \mu t$  and  $R = \mu^{1/2} r$  (in 1D) and consider them independently, which modifies the time and space derivatives as follows:

$$\partial / \partial t \rightarrow \partial / \partial \tau + \mu \partial / \partial \tau, \quad (12)$$

$$\partial / \partial r \rightarrow \partial / \partial R + \mu^{1/2} \partial / \partial R. \quad (13)$$

Another scaled time  $\tau_2 = \mu^{1/2} t$  can also be introduced in general [2,10]. In 2D, the second coordinate,  $r_2$ , is scaled as  $\mu^{1/4}$  (for stripes) [33]. For the sake of simplicity, we restrict our consideration to the simplest 1D-case (for Turing instability) and to only one scaled time,  $\tau$ .

All operators  $\mathbf{J}, \mathbf{H}, \mathbf{N}, \mathbf{Q}$  and  $\mathbf{S}$  in (5) are expanded in powers of  $\mu$ ; for example,

$$\mathbf{J} = \mathbf{J}_0 + \mu \mathbf{J}_1 + \mu^2 \mathbf{J}_2 + \dots, \quad (14)$$

where  $\mathbf{J}_0 = \mathbf{J}|_{\mu=0}$ . The expansion of  $\mathbf{X}$  with the lowest powers of  $\mu$  is:

$$\mathbf{X} = \mu^{1/2} \mathbf{X}_1 + \mu \mathbf{X}_2 + \mu^{3/2} \mathbf{X}_3 + \dots \quad (15)$$

This form follows from the structure of the spatial (12) and temporal (13) transformations.

Next, we substitute these expansions in Eq. (5) and collect all terms of the same power of  $\mu$ , which gives us a set of equations for the first ( $\mu^{1/2}$ ), second ( $\mu$ ) and third ( $\mu^{3/2}$ ) orders as:

$$\partial \mathbf{X}_1 / \partial t = (\mathbf{J}_0 + \mathbf{D}_0 \partial^2 / \partial r^2) \mathbf{X}_1 \equiv \mathbf{L}_0 \mathbf{X}_1, \quad (16)$$

$$(\partial / \partial t - \mathbf{L}_0) \mathbf{X}_2 = 2\mathbf{D}_0 \frac{\partial^2}{\partial r \partial R} \mathbf{X}_1 + \mathbf{H}_0 \mathbf{X}_1 \mathbf{X}_1 + \mathbf{Q} \left[ \mathbf{X}_1 \frac{\partial^2}{\partial r^2} \mathbf{X}_1 + \left( \frac{\partial \mathbf{X}_1}{\partial r} \right)^2 \right] \equiv \mathbf{I}_2, \quad (17)$$

$$(\partial / \partial t - \mathbf{L}_0) \mathbf{X}_3 = \mathbf{I}_3, \quad (18)$$

where

$$\mathbf{I}_3 \equiv -\partial \mathbf{X}_1 / \partial \tau + \mathbf{J}_1 \mathbf{X}_1 + \mathbf{D}_0 \frac{\partial^2}{\partial R^2} \mathbf{X}_1 + 2\mathbf{D}_0 \frac{\partial^2}{\partial r \partial R} \mathbf{X}_2 + 2\mathbf{H}_0 \mathbf{X}_1 \mathbf{X}_2 + \mathbf{N}_0 \mathbf{X}_1 \mathbf{X}_1 \mathbf{X}_1 + \mathbf{I}' + \mathbf{I}'', \quad (19)$$

$$\mathbf{I}' \equiv \mathbf{Q} \left[ \mathbf{X}_1 \frac{\partial^2}{\partial r^2} \mathbf{X}_2 + 2\mathbf{X}_1 \frac{\partial^2}{\partial r \partial R} \mathbf{X}_1 + \mathbf{X}_2 \frac{\partial^2}{\partial r^2} \mathbf{X}_1 + 2 \frac{\partial \mathbf{X}_1}{\partial r} \frac{\partial \mathbf{X}_2}{\partial r} + 2 \frac{\partial \mathbf{X}_1}{\partial r} \frac{\partial \mathbf{X}_1}{\partial R} \right], \quad (20)$$

$$\mathbf{I}'' \equiv \frac{1}{2} \mathbf{S} \left[ \mathbf{X}_1^2 \frac{\partial^2}{\partial r^2} \mathbf{X}_1 + 2\mathbf{X}_1 \left( \frac{\partial \mathbf{X}_1}{\partial r} \right)^2 \right]. \quad (21)$$

Eq. (16) is just the equation for the linear stability analysis of the homogeneous steady state. For Hopf and Turing instabilities, respectively, a solution  $\mathbf{X}_1$  of Eq. (16) can be found in the following form:

$$\mathbf{X}_1 = W(\tau, R) \mathbf{U} \exp(i\omega_c t) + \text{c.c.}, \quad (22)$$

$$\mathbf{X}_1 = W(\tau, R) \mathbf{U} \exp(ik_c r) + \text{c.c.}, \quad (23)$$

where  $W(\tau, R)$  is a complex amplitude that we need to determine,  $\mathbf{U}$  is the right eigenvector (the column vector) of matrix  $\mathbf{L}_0$ ,  $\omega_c$  and  $k_c$  are the critical frequency and

wavenumber, which are characteristic for the Hopf and Turing instabilities, respectively, and c.c. signifies complex conjugate.

A solution of Eq. (17),  $\mathbf{X}_2$ , may be sought in the general form of a linear combination of the zeroth, first and second subharmonics with coefficients  $V_i$ :

$$\mathbf{X}_2 = \mathbf{V}_0 + \mathbf{V}_1 \exp(i\omega_c t) + \mathbf{V}_2 \exp(2i\omega_c t) + \text{c.c.} , \quad (24)$$

$$\mathbf{X}_2 = \mathbf{V}_0 + \mathbf{V}_1 \exp(ik_c r) + \mathbf{V}_2 \exp(2ik_c r) + \text{c.c.} . \quad (25)$$

Note that the coefficients  $V_i$  depend on the amplitude  $W(\tau, R)$ .

Finally, the amplitude equation is just the *solvability condition* (Fredholm alternative) [34] for the third order [Eq. (18)] of our expansion:

$$\langle \mathbf{U}^* | \mathbf{I}_3 \rangle = 0 , \quad (26)$$

where the vector  $\mathbf{U}^*$  is the left eigenvector (row vector) of matrix  $\mathbf{L}_0$ . The right  $\mathbf{U}$  and left  $\mathbf{U}^*$  eigenvectors are determined from the eigenvalue problems

$$\mathbf{L}_0 \mathbf{U} = \lambda_0 \mathbf{U} \text{ and } \mathbf{U}^* \mathbf{L}_0 = \lambda_0 \mathbf{U}^* \quad (27)$$

as well as from the normalization condition

$$\mathbf{U}^* \mathbf{U} = \bar{\mathbf{U}}^* \bar{\mathbf{U}} = 1, \quad (28)$$

where the upper bar denotes the complex conjugate vector, and from the orthogonality condition

$$\mathbf{U}^* \bar{\mathbf{U}} = \bar{\mathbf{U}}^* \mathbf{U} = 0. \quad (29)$$

From Eq. (26), after doing some algebra, one can obtain the final form of the amplitude equation of type (2) for Hopf instability or (4) for Turing instability.

From (20) and (21) it can be seen that all terms in  $\mathbf{I}'$  and  $\mathbf{I}''$  contain derivatives with respect to  $r$ . For the case of Hopf instability, when the deviations  $\mathbf{X}_1$  [see Eq. (22)] and  $\mathbf{X}_2$  [see Eq. (24)] are independent of the spatial variable  $r$ , this means that both  $\mathbf{I}'$  and  $\mathbf{I}''$  vanish and  $\mathbf{I}_3$  is determined at the constant diffusion matrix  $\mathbf{D}_0 = \mathbf{D}(\mathbf{Z}_0)$ . Note also that in expression (19) for  $\mathbf{I}_3$ , the term  $2\mathbf{D}_0 \frac{\partial^2}{\partial r \partial R} \mathbf{X}_2$  vanishes, because  $\mathbf{X}_2$  is independent of  $r$ , while the term  $\mathbf{D}_0 \frac{\partial^2}{\partial R^2} \mathbf{X}_1$  produces the diffusion term in the CGLE [i.e.,  $(1 + ic_1)\nabla^2 W$ ].

### 3. Two-variable reaction-diffusion system with cross-diffusion terms

Now we can specify the procedure for obtaining the amplitude equations for a general two-variable reaction-diffusion system, since all coefficients of the CGLE and TAE can be found analytically in this case. For simplicity, we restrict our consideration to constant diffusion coefficients in the matrix  $\mathbf{D}_0$ . Then the general model (1) assumes the form

$$\partial u / \partial t = F_1(u, v) + D_{11} \partial^2 u / \partial r^2 + D_{12} \partial^2 v / \partial r^2, \quad (30)$$

$$\partial v / \partial t = F_2(u, v) + D_{21} \partial^2 u / \partial r^2 + D_{22} \partial^2 v / \partial r^2. \quad (31)$$

Introducing the deviation  $\mathbf{X} = \begin{pmatrix} x_u \\ x_v \end{pmatrix}$  from the steady state  $\mathbf{Z}_0 = \begin{pmatrix} u_0 \\ v_0 \end{pmatrix}$ , linearizing

(30), (31) around  $\mathbf{Z}_0$ , and assuming that deviation  $\mathbf{X}$  behaves as  $\exp(\lambda t + ikr)$ , we

obtain the eigenvalues  $\lambda$  of the matrix  $\mathbf{L} = \mathbf{J} + \mathbf{D}\nabla^2$  from the characteristic equation

$$\lambda^2 + \gamma(k)\lambda + \delta(k) = 0, \quad (32)$$

where  $\gamma(k) = -J_{11} - J_{22} + D_{11}k^2 + D_{22}k^2$  [ $-\gamma(k)$  is the trace of the matrix  $\mathbf{J} - k^2\mathbf{D}$ ] and

$$\delta(k) = (D_{11}k^2 - J_{11})(D_{22}k^2 - J_{22}) - (D_{12}k^2 - J_{12})(D_{21}k^2 - J_{21}) \quad (\text{determinant of } \mathbf{J} - k^2\mathbf{D}).$$

For the onset of Hopf instability, when  $\text{Re } \lambda = 0$  and  $\text{Im } \lambda \neq 0$ , at  $k = 0$ , we have

$\gamma(0) = 0$ . The conditions for the onset of Turing instability are:

$$\delta(k) = 0 \Rightarrow 2\lambda = -\gamma(k) + \sqrt{\gamma(k)^2 - 4\delta(k)} = 0 \quad (33)$$

and

$$d\delta(k)/dk = 0 \Rightarrow d\text{Re } \lambda / dk^2 = 0 \quad (34)$$

which gives the critical wavenumber

$$k_{cT} = (\det \mathbf{J} / \det \mathbf{D})^{1/4}. \quad (35)$$

Consider first the case of *Turing instability* arising as a control parameter  $\mu$  is

varied. The right eigenvector of the matrix  $\mathbf{L}_0 = \mathbf{L}|_{\mu=0}$  is

$$\mathbf{U} = \begin{pmatrix} U_u \\ U_v \end{pmatrix} = \begin{pmatrix} 1 \\ \alpha \end{pmatrix} \exp(ik_{cT}r), \quad (36)$$

where

$$\alpha = -\frac{J_{11}^0 - k_{cT}^2 D_{11}}{J_{12}^0 - k_{cT}^2 D_{12}} = -\frac{J_{21}^0 - k_{cT}^2 D_{21}}{J_{22}^0 - k_{cT}^2 D_{22}} \quad (37)$$

with  $J_{ij}^0$  being the  $ij$ -element of the Jacobian  $\mathbf{J}_0 = \mathbf{J}|_{\mu=0}$ . The left eigenvector is

$$\mathbf{U}^* = (U_u^*, U_v^*) = (1 + \alpha\beta)^{-1} (1, \beta) \exp(ik_{cT}r), \quad (38)$$

where

$$\beta = -\frac{J_{11}^0 - k_{cT}^2 D_{11}}{J_{21}^0 - k_{cT}^2 D_{21}} = -\frac{J_{12}^0 - k_{cT}^2 D_{12}}{J_{22}^0 - k_{cT}^2 D_{22}}. \quad (39)$$

The vector  $\mathbf{X}$  can be expanded as [see Eq. (15)]:

$$\begin{pmatrix} x_u \\ x_v \end{pmatrix} = \mu^{1/2} \begin{pmatrix} x_{u1} \\ x_{v1} \end{pmatrix} + \mu \begin{pmatrix} x_{u2} \\ x_{v2} \end{pmatrix} + \dots \quad (40)$$

The first and second terms of (40) have the forms [see Eqs. (23) and (25)]

$$\begin{pmatrix} x_{u1} \\ x_{v1} \end{pmatrix} = \begin{pmatrix} 1 \\ \alpha \end{pmatrix} W(\tau, R) \exp(ik_{cT}r) + \text{c.c.}, \quad (41)$$

$$\begin{pmatrix} x_{u2} \\ x_{v2} \end{pmatrix} = \begin{pmatrix} a_0 \\ b_0 \end{pmatrix} + \begin{pmatrix} a_1 \\ b_1 \end{pmatrix} \exp(ik_{cT}r) + \begin{pmatrix} a_2 \\ b_2 \end{pmatrix} \exp(2ik_{cT}r) + \text{c.c.}. \quad (42)$$

Here  $a_i$  and  $b_i$ ,  $i = 0, 1, 2$ , are the components of the vectors  $V_i$  in Eq. (25). We can find them from the  $\mu$ -order term of the expansion. The coefficients  $a_0$  and  $b_0$  in (42) are determined as

$$a_0 = -\frac{2}{\det \mathbf{J}_0} (G_1 J_{22}^0 - G_2 J_{12}^0) |W|^2 \quad (43)$$

$$b_0 = -\frac{2}{\det \mathbf{J}_0} (G_2 J_{11}^0 - G_1 J_{21}^0) |W|^2, \quad (44)$$

where

$$G_i = \frac{1}{2} H_i^{uu} + \alpha H_i^{uv} + \frac{\alpha^2}{2} H_i^{vv}. \quad (45)$$

Here the subscript denotes the component ( $i = 1, 2$ ), whereas the superscripts denote derivatives with respect to the corresponding variables, so, for example

$$H_i^{uv} = \left. \frac{\partial^2 F_i(u, v)}{\partial u \partial v} \right|_{u_0, v_0; \mu=0}, \quad N_i^{uv} = \left. \frac{\partial^3 F_i(u, v)}{\partial u^2 \partial v} \right|_{u_0, v_0; \mu=0}. \quad (46)$$

The  $\exp(ik_{cT}r)$  term yields the combination of coefficients  $a_1$  and  $b_1$  as

$$\alpha a_1 - b_1 = 2ik_{\text{cT}} \frac{D_{11} + \alpha D_{12}}{J_{12}^0 - k_{\text{cT}}^2 D_{12}} \frac{\partial W}{\partial R} = 2ik_{\text{cT}} \frac{D_{21} + \alpha D_{22}}{J_{22}^0 - k_{\text{cT}}^2 D_{22}} \frac{\partial W}{\partial R}. \quad (47)$$

From (47) and (39) it follows that  $D_{11} + \alpha D_{12} + \beta D_{21} + \alpha\beta D_{22} = 0$  so that the term

$\mathbf{D}_0(\partial^2 \mathbf{X}_1 / \partial R^2)$  in Eq. (19) vanishes after applying the Fredholm alternative. The last coefficients,  $a_2$  and  $b_2$ , appear in the  $\exp(2ik_{\text{cT}}r)$  term and read

$$a_2 = \frac{1}{\det \varphi} (G_1 \varphi_{22} - G_2 \varphi_{12}) W^2, \quad (48)$$

$$b_2 = \frac{1}{\det \varphi} (G_2 \varphi_{11} - G_1 \varphi_{21}) W^2, \quad (49)$$

where  $\varphi_{ij} = -J_{ij}^0 + 4k_{\text{cT}}^2 D_{ij}$ .

Finally, using the Fredholm alternative (26) rewritten in the two-component form

$U_u^* I_{3u}^+ + U_v^* I_{3v}^+ = 0$  with  $\mathbf{I}_3$  expressed as

$$\mathbf{I}_3 = \begin{pmatrix} I_{3u} \\ I_{3v} \end{pmatrix} = \begin{pmatrix} I_{3u}^+ \\ I_{3v}^+ \end{pmatrix} \exp(ik_{\text{cT}}r) + \begin{pmatrix} I_{3u}^- \\ I_{3v}^- \end{pmatrix} \exp(-ik_{\text{cT}}r) + \text{terms of other orders of } r, \quad (50)$$

where the deviations (40) – (42) are inserted in (19), we obtain the amplitude equation in the form of Eq. (4) with the derivatives now with respect to  $\tau$  and  $R$  instead of  $t$  and  $r$ ,

where

$$\eta = \eta_{\text{T}} = \frac{1}{1 + \alpha\beta} (J_{11}^1 + \alpha J_{12}^1 + \beta J_{21}^1 + \alpha\beta J_{22}^1), \quad (51)$$

$$D_{\text{T}} = 4k_{\text{cT}}^2 \frac{D_{21} + \alpha D_{22}}{1 + \alpha\beta} \frac{D_{12} + \beta D_{22}}{J_{22}^0 - k_{\text{cT}}^2 D_{22}}, \quad (52)$$

$$\begin{aligned}
g &= \hat{g} / (1 + \alpha\beta), \\
\hat{g} &= (H_1^{uu} + \beta H_2^{uu} + \alpha H_1^{uv} + \alpha\beta H_2^{uv}) \left[ -\frac{2}{\det \mathbf{J}_0} (G_1 J_{22}^0 - G_2 J_{12}^0) + \frac{1}{\det \varphi} (G_1 \varphi_{22} - G_2 \varphi_{12}) \right] + \\
& (H_1^{vv} + \beta H_2^{vv} + \alpha H_1^{uv} + \alpha\beta H_2^{uv}) \left[ -\frac{2}{\det \mathbf{J}_0} (G_2 J_{11}^0 - G_1 J_{21}^0) + \frac{1}{\det \varphi} (G_2 \varphi_{11} - G_1 \varphi_{21}) \right] + \\
& \frac{1}{2} \left[ (N_1^{uuu} + \beta N_2^{uuu}) + 3\alpha (N_1^{uuv} + \beta N_2^{uuv}) + 3\alpha^2 (N_1^{uvv} + \beta N_2^{uvv}) + \alpha^3 (N_1^{vvv} + \beta N_2^{vvv}) \right]
\end{aligned} \tag{53}$$

and

$$J_{ij}^1 = \left. \frac{dJ_{ij}}{d\mu} \right|_{\mu=0} \tag{54}$$

for the elements of the matrix  $\mathbf{J}_1$ .

In general, the TAE (4) can be rescaled if we perform the transformations:

$\mu \partial / \partial \tau \rightarrow \partial / \partial t$ ,  $\mu^{1/2} \partial / \partial R \rightarrow \partial / \partial r$  and  $\mu W \rightarrow W$  [12,14]. From (51) – (53), we can see

that the effect of cross-diffusion appears in all coefficients  $\eta_T, D_T$  and  $g$  of the TAE,

since  $\alpha$  and  $\beta$  (which determine the right and left eigenvectors) depend on  $D_{12}$  and/or

$D_{21}$ .

Now let us consider *Hopf instability*. The same result for the amplitude equations in the Hopf case may be obtained using Kuramoto's procedure [5,9]. The equivalence of our manipulations to Kuramoto's formulation is shown in [Appendix A](#). Therefore, we use his method to calculate the coefficient of the cubic term in the CGLE, because only the coefficient  $c_1$  of the CGLE (2) depends on cross-diffusion, while  $c_0$  and  $c_2$  are the same as in the case of no diffusion. To find  $c_1$ , we must calculate the eigenvectors  $\mathbf{U}^*$  and  $\mathbf{U}$  of  $\mathbf{J}_0$ , which has a pure imaginary eigenvalue  $i\omega_0$  in the case of the Hopf instability.

Due to the specific properties of  $\mathbf{J}_0$  for the Hopf case, we have two relationships between its elements  $J_{ij}$  (here we have dropped the 0 -superscript in  $J_{ij}^0$  for simplicity):

$$J_{11} = -J_{22} \quad (55)$$

and

$$\omega_0^2 = -J_{11}^2 - J_{12}J_{21}. \quad (56)$$

Now we can obtain the eigenvectors  $\mathbf{U}^*$  and  $\mathbf{U}$ :

$$\mathbf{U}^* = \frac{1}{2} \begin{pmatrix} -i \frac{J_{11}}{\omega_0}, & \frac{J_{11}}{J_{21}} + i \frac{J_{11}^2}{J_{21}\omega_0} \end{pmatrix}, \quad \mathbf{U} = \begin{pmatrix} 1 + i\omega_0 / J_{11} \\ J_{21} / J_{11} \end{pmatrix} \quad (57)$$

We can then calculate  $\mathbf{U}^* \mathbf{D} \mathbf{U} = d' + id''$ , which gives  $c_1$  in general form as:

$$c_1 = d'' / d' = \frac{1}{\omega_0} \frac{J_{11}(D_{22} - D_{11}) - J_{21}D_{12} - J_{12}D_{21}}{D_{11} + D_{22}}. \quad (58)$$

We see here that the contribution of the cross-diffusion terms,  $D_{12}$  and  $D_{21}$ , to  $c_1$  depends on the sign (and absolute value) of the elements  $J_{21}$  and  $J_{12}$ , respectively.

In the next two sections we apply the general equations deduced here to the Oregonator and Brusselator models.

#### 4. Oregonator model

For the two-variable Oregonator model, the functions  $F_1(u, v)$  and  $F_2(u, v)$  in Eqs. (30) and (31) are specified as  $F_1(u, v) = [u - u^2 - fv(u - q) / (u + q)] / \varepsilon$  and  $F_2(u, v) = u - v$  [20,21]; the parameters  $f, q, \varepsilon, D_{ij}$  are positive constants,  $D_{22}$  can be chosen to be 1 for

the normalized case, but we keep the notation  $D_{22}$  for generality. The steady state solution,  $(u_0, v_0)$ , satisfies  $F_1(u_0, v_0) = F_2(u_0, v_0) = 0$  and reads

$$u_0 = v_0 = (1/2) \left[ 1 - q - f + \sqrt{(1 - q - f)^2 + 4q(1 + f)} \right]. \quad (59)$$

The elements of the Jacobian matrix  $\mathbf{J}$  are

$$J_{11} = \partial F_1(u, v) / \partial u = \left[ 1 - 2u_0 - 2qfv_0 / (u_0 + q)^2 \right] / \varepsilon,$$

$$J_{12} = \partial F_1(u, v) / \partial v = -(f / \varepsilon)(u_0 - q) / (u_0 + q), \quad J_{21} = \partial F_2(u, v) / \partial u = 1,$$

$$J_{22} = \partial F_2(u, v) / \partial v = -1$$

calculated at  $u = u_0$  and  $v = v_0$ .

For the onset of Hopf instability, the critical value  $\varepsilon_{\text{CH}}$  of the parameter  $\varepsilon$  can be expressed as a function of  $q$  and  $f$  [using the general Eq. (55)]:

$$\varepsilon_{\text{CH}} = 1 - 2u_0 - \frac{2qfv_0}{(u_0 + q)^2}. \quad (60)$$

At the onset of Hopf instability,  $\text{Im}(\lambda_0) = \omega_0$ , the frequency  $\omega_0$  can be found from eqs.

(56) and (60) as

$$\omega_0^2 = (1 - u_0) / \varepsilon_{\text{CH}} - 1. \quad (61)$$

We consider the situation when, as we decrease  $\varepsilon$ , the Hopf instability occurs before the Turing instability. The conditions for the onset of Turing instability yield the critical value  $\varepsilon_{\text{CT}}$  at the critical wavenumber  $k_{\text{CT}}$  [given by Eq. (35)] as

$$\varepsilon_{\text{CT}} = \left[ -b + \sqrt{b^2 - 4ac} \right]^2 / (4a^2), \quad (62)$$

where  $a = D_{11} + D_{12}$ ,  $b = \sqrt{-4(j_{11} + j_{12}) \det \mathbf{D}}$ , and  $c = j_{12}D_{21} - j_{11}D_{22}$ ,  $\sqrt{\varepsilon_{\text{CT}}} > 0$  and

$$j_{12} \equiv \varepsilon J_{12} = f(q - u_0) / (q + u_0), \quad (63)$$

$$j_{11} \equiv \varepsilon J_{11} = 1 - 2u_0 - 2qfv_0 / (q + u_0)^2. \quad (64)$$

When the Hopf instability occurs before the Turing instability,

$$\varepsilon_{\text{cH}} > \varepsilon_{\text{cT}}. \quad (65)$$

**CGLE for the Oregonator model.** First we introduce a small control parameter  $\mu$ :

$$\mu = (\varepsilon - \varepsilon_{\text{cH}}) / \varepsilon_{\text{cH}}. \quad (66)$$

Then we calculate  $\mathbf{J}_0$  and  $\mathbf{J}_1$ :

$$\mathbf{J}_0 = \begin{pmatrix} 1 & -1 - \omega_0^2 \\ 1 & -1 \end{pmatrix}, \quad (67)$$

$$\mathbf{J}_1 = \left. \frac{d\mathbf{J}}{d\varepsilon} \frac{d\varepsilon}{d\mu} \right|_{\varepsilon=\varepsilon_{\text{cH}}} = \begin{pmatrix} -1 & \frac{1-u_0}{\varepsilon_{\text{cH}}} \\ 0 & 0 \end{pmatrix} \quad (68)$$

and find the left and right eigenvectors of  $\mathbf{J}_0$  [using Eq. (57)]:

$$\mathbf{U}^* = \frac{1}{2} \begin{pmatrix} -i \\ \omega_0 \end{pmatrix}, \quad 1 + \frac{i}{\omega_0}, \quad \mathbf{U} = \begin{pmatrix} 1 + i\omega_0 \\ 1 \end{pmatrix}. \quad (69)$$

Using (68) and (69), we compute the combination  $\mathbf{U}^* \mathbf{J}_1 \mathbf{U} = \lambda_1 \equiv \sigma_1 + i\omega_1 = -(1/2)(1 + i\omega_0)$  and then find the coefficient  $c_0$  in the CGLE (2) as [9]

$$c_0 \equiv \omega_1 / \sigma_1 = \omega_0. \quad (70)$$

Next we determine the coefficient  $c_1$  from (58):

$$c_1 = \frac{1}{\omega_0} \frac{D_{22} - D_{11} - D_{12} + D_{21}(1 + \omega_0^2)}{D_{11} + D_{22}}. \quad (71)$$

Finally we find  $c_2 = g'' / g'$  following Kuramoto's procedure, which is rather cumbersome and is detailed in [Appendix B](#).

The CGLE is valid only at  $g' > 0$ , when the Hopf bifurcation is supercritical. The dependence of the critical value  $f_c$  [ $f_c$  is the value of  $f$  at which  $g'$  changes sign from negative (at  $f < f_c$ ) to positive (at  $f > f_c$ )] on  $q$  is shown in Fig. 1a. Note that this dependence does not coincide with the dependence  $f_c' = 1 - q$  used in Ref. [17] as the boundary between super- and subcritical Hopf bifurcation.

Using the coefficients  $c_1$  and  $c_2$ , we identify regions with specific dynamical behaviors of the reaction-diffusion system, such as the domain of Benjamin-Feir instability (chemical turbulence), where  $1 + c_1 c_2 < 0$  [9], and domains of waves and antiwaves (phase waves propagating away from and toward a source of perturbation, respectively) [35,36]. The transition from wave (W) to antiwave (AW) behavior occurs when  $c_1 + c_2 = 0$  [16,17,37]. However, some works [16,17,37] use a different sign for  $ic_2$  in the term  $(1 + ic_2)|W|^2 W$  of the CGLE, which may lead to confusion, with the transition criterion then being  $c_1 - c_2 = 0$  instead of  $c_1 + c_2 = 0$ . Therefore, we carefully checked both criteria by direct numerical calculations with the original Oregonator reaction-diffusion model and conclude that the criterion  $c_1 + c_2 > (<)0$  corresponds to the AW (W) domain. In Fig. 1a, these two domains, W and AW, are plotted in the  $q - f$  parameter plane. Note that the necessary conditions for the validity of the CGLE, such as  $1 - u_0 > \varepsilon_{\text{CH}} > \varepsilon_{\text{CT}}$  are always fulfilled [see Eqs. (61) and (65)].

To illustrate the effect of cross-diffusion terms on the dynamic behavior of the system, the  $C_d - f$  parameter plane can be selected, where  $C_d \equiv D_{21}(1 + \omega_0^2) - D_{12}$  [see Eq. (71)] is the cross-diffusion contribution to  $c_1$ . First, we consider the case of  $D_{21} = 0$

(in which case  $C_d = -D_{12}$ ). In Fig. 1b we exhibit three domains: W, AW, and BF (Benjamin-Feir turbulence), which are plotted at two different values of  $D_{11}$ . As is seen in Fig. 1b, the transition between the W and AW domains can be induced by changing  $D_{12}$  in a rather broad range of  $f$ . In a relatively narrow range of  $f$  close to  $f_c$ , an increase in  $D_{12}$  can lead to transitions from AW to W and further to the BF domain. The interplay of both cross-diffusion coefficients can easily be seen by inserting  $c_1$  from (71) into the criterion for BF instability,  $1 + c_1 c_2 < 0$ ,

$$D_{21} < \frac{1}{1 + \omega_0^2} \left[ D_{11} + D_{12} - D_{22} - \frac{\omega_0}{c_2} (D_{11} + D_{22}) \right] \quad (72)$$

and into the criterion for AW,  $c_1 + c_2 > 0$ ,

$$D_{21} > \frac{1}{1 + \omega_0^2} [D_{11} + D_{12} - D_{22} - c_2 \omega_0 (D_{11} + D_{22})]. \quad (73)$$

Here we recall that  $c_2$  is independent of the diffusion coefficients. Therefore, the BF and AW regions in the  $(D_{12}, D_{21})$  plane are bounded by parallel straight lines which correspond to the equalities in (72) and (73). Note that if  $c_2 = \pm 1$ , the two lines coincide. At  $-1 < c_2 < 0$  or  $c_2 > 1$ , there is no W-domain, since this domain then overlaps with the BF domain, and the resulting waves are turbulent. The three domains, W, AW, and BF, are shown in Fig. 1c for  $0 < c_2 < 1$ .

In Fig. 1d we show the various behavioral domains in the  $D_{21}$ - $f$  plane at  $D_{11} = D_{22} = 1$  and  $D_{12} = 0$  [in which case  $C_d = D_{21}(1 + \omega_0^2)$ ]. We see that in addition to a region of BF instability close to  $f \cong 1$ , which exists at vanishing  $D_{21}$  and  $D_{12}$ , a new region of BF instability at large  $f$  ( $\approx 2$  and larger) emerges, which cannot be obtained at  $D_{21} = D_{12} = 0$ .

Note also that the analogous BF region exists for the case of  $D_{21} = 0$  (Fig. 1b), but only at much larger positive values of  $D_{12}$  ( $> 2$ ). Figures 1b and 1d should be mirror-symmetric with a “magnification factor”  $(1 + \omega_0^2)$ , since in the first case  $C_d = -D_{12}$ , while in the second  $C_d = D_{21}(1 + \omega_0^2)$ .

Examples of waves and antiwaves in the 1D case are shown in Fig. 2. In these computer experiments, a small portion at the left of the 1D segment was perturbed initially, starting from the homogeneous steady state (SS). In both W and AW, a wave packet propagates slowly to the right with the group velocity. In the case of AW (left column of Fig. 2), after sufficient time bulk oscillations start in the right portion of the system. In case of W (right column of Fig. 2) the right (unperturbed) portion of the 1D segment remains in the SS. In both cases, the boundary between the wave packet and either the bulk oscillations or the quiescent region moves slowly to the right. The bottom sections of Fig. 2 show the wave amplitudes.

Since the CGLE is applicable both the 1D and 2D cases, waves (antiwaves) found in 1D should correspond to circular waves (antiwaves) in 2D. To demonstrate this, we show in Fig. 3 examples of circular waves and antiwaves in 2D.

**TAE for the Oregonator model.** To analyze the Turing bifurcation, we introduce a new small control parameter  $\mu$  as we did in Eq. (66), replacing  $\varepsilon_{\text{CH}}$  by  $\varepsilon_{\text{CT}}$ . The eigenvectors  $\mathbf{U}$  [given by (36)] and  $\mathbf{U}^*$  [given by (38)] are now specified by

$$\alpha = \frac{k_{\text{CT}}^2 D_{11} - j_{11} / \varepsilon_{\text{CT}}}{j_{12} / \varepsilon_{\text{CT}} - k_{\text{CT}}^2 D_{12}}, \quad (74)$$

$$\beta = \frac{j_{12} / \varepsilon_{\text{CT}} - k_{\text{CT}}^2 D_{12}}{1 + k_{\text{CT}}^2 D_{22}} = -\frac{j_{11} / \varepsilon_{\text{CT}} - k_{\text{CT}}^2 D_{11}}{1 - k_{\text{CT}}^2 D_{21}}, \quad (75)$$

where  $j_{11}$  and  $j_{12}$  are given by (64) and (63), respectively. Note that Eq. (75) can be solved for  $\varepsilon_{\text{cT}}$  as

$$\varepsilon_{\text{cT}} = \frac{j_{11}/k_{\text{cT}}^2 + j_{12}/k_{\text{cT}}^2 + j_{11}D_{22} - j_{12}D_{21}}{D_{11} + D_{12} + k_{\text{cT}}^2 \det \mathbf{D}}. \quad (76)$$

If we know  $k_{\text{cT}}$  from (35), then we can find  $\varepsilon_{\text{cT}}$  using (76) instead of (62). Applying the general equations (51)-(54) for the Oregonator model, we obtain the following coefficients for the final form of the TAE (4):

$$\eta = \eta_{\text{T}} = -\frac{1}{\varepsilon_{\text{cT}}} \frac{j_{11} + \alpha j_{12}}{1 + \alpha\beta}, \quad (77)$$

$$D_{\text{T}} = -4k_{\text{cT}}^2 \frac{D_{21} + \alpha D_{22}}{1 + \alpha\beta} \frac{D_{12} + \beta D_{22}}{1 + k_{\text{cT}}^2 D_{22}}, \quad (78)$$

$$\begin{aligned} g = \hat{g} / (1 + \alpha\beta), \quad \hat{g} = H_1^{uu} (H_1^{uu} + 2\alpha H_1^{uv}) & \left[ \frac{1}{2(\varphi_1 - \chi\varphi_2)} - \frac{\varepsilon_{\text{cT}}}{j_{11} + j_{12}} \right] + \\ H_1^{uv} (H_1^{uu} + 2\alpha H_1^{uv}) & \left[ \frac{1}{2(\varphi_1 - \chi\varphi_2)} (\alpha + \chi) - \frac{\varepsilon_{\text{cT}}}{j_{11} + j_{12}} (1 + \alpha) \right] + (N_1^{uuu} + 3\alpha N_1^{uuv}) / 2, \end{aligned} \quad (79)$$

where

$$\varphi_1 = -j_{11} / \varepsilon_{\text{cT}} + 4k_{\text{cT}}^2 D_{11}, \quad (80)$$

$$\varphi_2 = j_{12} / \varepsilon_{\text{cT}} - 4k_{\text{cT}}^2 D_{12}, \quad (81)$$

$$\chi = \frac{1 - 4k_{\text{cT}}^2 D_{21}}{1 + 4k_{\text{cT}}^2 D_{22}} \quad (82)$$

and the Hessian elements  $H_1^{uu}$  and  $H_1^{uv}$  and the elements  $N_1^{uuu}$  and  $N_1^{uuv}$  are given in [Appendix B](#) [Eqs. (B3) and (B6)] for the CGLE with the provision that  $\varepsilon_{\text{cH}}$  must be replaced by  $\varepsilon_{\text{cT}}$ .

In [Figure 4](#), we display several parameter planes, showing regions of Turing instability as calculated from the TAE for the Oregonator. The sign of  $g$  in a region determines whether the instability is supercritical ( $g < 0$ ) or subcritical ( $g > 0$ ). From [Fig. 4c](#) and [4d](#) we observe that to obtain Turing instability when  $D_{11} = D_{22} = 1$ ,  $D_{21}$  should be positive (repulsion of inhibitor from areas of concentrated activator) and  $D_{12}$  negative (attraction of activator to regions of concentrated inhibitor). In all parameter planes there is a line close to  $f = 1$  separating regions of super- and sub-critical Turing instability. A second such boundary can be seen at larger  $f$  in [Fig. 4a - 4c](#), the position of which strongly depends on the diffusion coefficients.

## 5. Brusselator model

For the Brusselator model [22] with cross-diffusion terms described by Eqs. (30), (31), the functions  $F_1$  and  $F_2$  are  $F_1(u, v) = A - (B + 1)u + u^2v$  and  $F_2(u, v) = Bu - u^2v$ . The critical value of the control parameter  $B$  at the Hopf instability is  $B_{\text{cH}} = 1 + A^2$ . The critical wavenumber  $k_c$  for the onset of Turing instability is determined from Eq. (35) as

$$k_c^2 = A / \sqrt{\det \mathbf{D}} \quad (83)$$

while the critical parameter  $B_{\text{cT}}$  is found from Eq. (33) using Eq. (83) and is given by

$$B_{\text{cT}} = \left[ A^2 (D_{11} + D_{21}) + 2A\sqrt{\det \mathbf{D}} + D_{22} \right] / (D_{12} + D_{22}). \quad (84)$$

To calculate the coefficients of the CGLE and TAE, we employ below these expressions for  $k_c^2$  and  $B_{\text{cT}}$ .

**CGLE for the Brusselator model.** The CGLE for the Brusselator model without cross-diffusion terms has been derived elsewhere [9,14], and we present here only the main results relevant to the case of cross-diffusion. First, we choose the critical small parameter  $\mu$  :

$$\mu = \frac{B - B_{\text{cH}}}{B_{\text{cH}}}. \quad (85)$$

Then we find the operator  $\mathbf{J}_0$  :

$$\mathbf{J}_0 = \begin{pmatrix} A^2 & A^2 \\ -(1 + A^2) & -A^2 \end{pmatrix}. \quad (86)$$

and calculate the coefficient  $c_1$  from (58):

$$c_1 = \omega_0 \frac{D_{22} - D_{11} - D_{21} + D_{12}(1 + 1/\omega_0^2)}{D_{11} + D_{22}}. \quad (87)$$

For the Brusselator model, we have  $\omega_0 = A$ . The coefficient  $c_2 = g''/g'$  is independent of the diffusion coefficients and is given in Ref. [9]:

$$c_2 = \frac{4 - 7A^2 + 4A^4}{3A(2 + A^2)}. \quad (88)$$

Note that  $g' = (2 + A^2)/(2A^2)$  is always positive, and hence the Hopf bifurcation in the Brusselator model is always supercritical, so that we can write the CGLE for any value of  $A$ . The coefficient  $c_0$  is derived from  $\mathbf{U}^* \mathbf{J}_1 \mathbf{U} = \lambda_1 \equiv \sigma_1 + i\omega_1$  as  $c_0 = \omega_1 / \sigma_1 = 0$ ,

where  $\mathbf{J}_1 = (1 + A^2) \begin{pmatrix} 1 & 0 \\ -1 & 0 \end{pmatrix}$  and  $\sigma_1 = (1 + A^2)/2, \omega_1 = 0$ .

We plot the W, AW, and BF domains in two parametric planes:  $(A - D_{11})$  at  $D_{12} = D_{21} = 0$  (Fig. 5a) and  $(A - C_d)$  [ $-C_d \equiv D_{21} - D_{12}(1 + 1/\omega_0^2)$  and  $-C_d = D_{21}$  at  $D_{12} = 0$ ] (Fig. 5b and 5d). As can be seen in Fig. 5d, at large enough  $-C_d$  (or large  $D_{21}$  at  $D_{12} = 0$ ), BF instability occurs, while at small enough  $-C_d$  ( $< -1$ ), there is an AW domain. The domain of waves (W) is squeezed between the AW and BF domains and exists only in a rather narrow range of the parameter  $A$  (approximately between 0.4 and 2). The minimum of the curve separating the W and AW domains and the maximum of the curve separating the W and BF domains correspond to  $A = 1$ . From Fig. 5b we can also conclude that if  $D_{11}$  is small enough ( $< 1$ ), only AW may be found in the Brusselator model at  $D_{21} = D_{12} = 0$ . Examples of BF turbulence and AW in the Brusselator model are shown in Fig. 6.

**TAE for the Brusselator model.** The TAE for the Brusselator model without cross-diffusion terms was obtained earlier [12,14]. Here we present the TAE for the Brusselator model with cross-diffusion. The control parameter  $\mu$  is introduced as

$$\mu = \frac{B - B_{cT}}{B_{cT}}. \quad (89)$$

The TAE (4) has the following coefficients

$$\eta = \eta_B = (A/\Psi_1)(D_{12} + D_{22})^2(B - B_{cT}), \quad (90)$$

$$g = (A/\Psi_1)(D_{12} + D_{22})(\Psi_2 + \Psi_3), \quad (91)$$

$$D_T = D_B = 4(A/\Psi_1)(D_{12} + D_{22}) \det \mathbf{D}, \quad (92)$$

where

$$\Psi_1 = A(D_{12} + D_{22})\left(A\sqrt{\det \mathbf{D}} + D_{22}\right) - \left(A\sqrt{\det \mathbf{D}} - D_{12}\right)\left[A(D_{11} + D_{21}) + \sqrt{\det \mathbf{D}}\right], \quad (93)$$

$$\Psi_2 = -\frac{2}{9A^3\sqrt{\det \mathbf{D}}}\left[D_{22} - A^2(D_{11} + D_{21})\right]\left[4A^2(D_{11} + D_{21}) + 15A\sqrt{\det \mathbf{D}} - 4D_{22}\right], \quad (94)$$

$$\Psi_3 = -\frac{3}{A}\left[A(D_{11} + D_{21}) + \sqrt{\det \mathbf{D}}\right]. \quad (95)$$

If  $D_{12} = D_{21} = 0$  (no cross-diffusion), we recover from (90) – (95) the amplitude equation obtained by De Wit and Walgraef [12,14].

If  $g$  is positive, the Turing instability is subcritical. In Fig. 7 we show the regions of super- and subcritical Turing instability. The condition  $g = 0$  is determined by the equation  $\Psi_2 + \Psi_3 = 0$  [see Eq. (91)]. This expression can be rewritten as

$$\begin{aligned} & 2[D_{22} - A^2(D_{11} + D_{21})]\left[4A^2(D_{11} + D_{21}) + 15A\sqrt{\det \mathbf{D}} - 4D_{22}\right] + \\ & 27A^2\sqrt{\det \mathbf{D}}\left[A(D_{11} + D_{21}) + \sqrt{\det \mathbf{D}}\right] = 0. \end{aligned} \quad (96)$$

If  $D_{21} = 0$ , then  $\det \mathbf{D} = D_{11}D_{22}$  and Eq. (96) is independent of  $D_{12}$ , i.e., the super/subcritical areas are separated in the  $(A - D_{21})$  plane by the straight (bold horizontal) lines in Fig. 7a. When  $D_{11} = D_{22} = 1$  and  $D_{21} = 0$ , we can find from (96) two values,  $A = (21 \pm \sqrt{313})/16$  ( $\cong 2.418$  and  $0.207$ ), that correspond to the two horizontal straight lines in Fig. 7a.

If  $D_{12} = 0$ , then we can find from Eq. (96) an expression for  $D_{21}$  at which  $g = 0$ :

$$D_{21} = -D_{11} + \frac{1}{16A^2}\left[16D_{22} - 3A\sqrt{D_{11}D_{22}} \pm 3\sqrt{A\sqrt{D_{11}D_{22}}\left(96D_{22} + 97A\sqrt{D_{11}D_{22}}\right)}\right]. \quad (97)$$

Eq. (97) gives the two branches of the boundary between the sub- and supercritical Turing domains (shown in Fig. 7b). These lines tend to infinity if  $D_{21}$  approaches  $-D_{11}$ .

## 6. Discussion and conclusion

We can now summarize the effects of constant cross-diffusion coefficients on the system behavior close to the onset of Hopf or Turing instability. For the CGLE (Hopf instability), cross-diffusion affects only the linear coefficient,  $c_1$ , whereas the cubic coefficient  $c_2$  is independent of diffusion terms.

One can see that the cross-diffusion coefficients  $D_{12}$  and  $D_{21}$  contribute to  $c_1$  asymmetrically both in the Oregonator and Brusselator models. For the Oregonator model, increasing  $D_{21}$  increases  $c_1$ , while raising  $D_{12}$  decreases  $c_1$ . The opposite effect of  $D_{12}$  and  $D_{21}$  on  $c_1$  occurs in the Brusselator model. This behavior can be understood from Eq. (58), which shows that the effect of  $D_{12}$  and  $D_{21}$  on  $c_1$  is proportional to the Jacobian matrix elements  $J_{21}$  and  $J_{12}$ , respectively. Although the instability in both models is of the “direct autocatalysis” type as defined by Tyson [38], examination of Eqs. (67) and (86) shows that the community matrix, which consists of the signs of the elements of  $\mathbf{J}_0$  at the critical point, is  $\begin{pmatrix} + & - \\ + & - \end{pmatrix}$  for the Oregonator and  $\begin{pmatrix} + & + \\ - & - \end{pmatrix}$  for the Brusselator.

Varying the coefficient  $c_1$  shifts the boundary between the wave and anti-wave domains and can lead to the emergence of new behavior, such as BF instability, both in the Oregonator and Brusselator models. For the Oregonator model, however, in the region of BF instability (at  $f \approx 1$ ), our simulations produced chaotic waves only at some parameters, while at other parameters in the same domain no such behavior was found. It

is possible that proximity of a subcritical Hopf region may be responsible for this anomalous behavior. It has also been suggested [26] that, because the Oregonator model contains quite different characteristic time scales, it may be badly described by the CGLE even in the vicinity of the Hopf bifurcation.

In the case of the Belousov-Zhabotinsky reaction, the link between the parameters of the reaction-diffusion system and the constants of the Oregonator CGLE may allow us to identify conditions under which unusual dynamic behavior may occur. For example, if  $c_1 = c_2 = 0$ , both the group and phase velocities of waves are zero [16]. If we perturb the SS locally, then a pseudo-oscillon can emerge, i.e., a localized spot that oscillates for many periods while the remainder of the system is quiescent. We refer to this phenomenon as a “pseudo-oscillon,” because this oscillon is not stable like a true oscillon [39], but rather spreads very slowly. For the Oregonator model, one such set of parameters is  $f = 1.693$ ,  $q = 0.001$ ,  $\varepsilon = 0.438$ ,  $D_{11} = 0.5$ ,  $D_{22} = 1$ ,  $D_{12} = 0.0481$ , and  $D_{21} = -0.2$ . The presence of cross-diffusion coefficients helps to find this special point by tuning  $D_{12}$  or  $D_{21}$ . At  $D_{11} = D_{22} = 1$  and  $D_{12} = D_{21} = 0$  such a point always exists, since  $c_1 = 0$  at  $D_{11} = D_{22}$  and the function  $c_2(f, q)$  has roots at some  $f$  and  $q$ , for example, at  $f \cong 1.722$  and  $q = 0.01$ , provided that  $\varepsilon$  is given by Eq. (60).

In the case of Turing instability the cross-diffusion coefficients contribute to all the coefficients,  $\eta$ ,  $D_T$ , and  $g$ , of the amplitude equation, but we have focused here on the effect of  $D_{ij}$  on  $g$ , i.e., on the boundary between supercritical and subcritical Turing instability. From Fig. 4 and Fig. 7, we observe that  $D_{12}$  in the Oregonator and  $D_{21}$  in the Brusselator model strongly affect the position of this boundary, while the other cross-diffusion coefficients have relatively little effect.

Note also that for non-zero cross-diffusion coefficients, it is possible in general for  $\det \mathbf{D}$  to approach zero. In this case,  $k_{cT}$  becomes very large [see Eq. (35)], and consequently the characteristic wavelength of Turing patterns,  $2\pi/k_{cT}$ , can be vanishingly small. We also note that Turing instability can occur even with  $D_{11} = D_{22}$ , if we have cross-diffusion (see Figs. 4 and 7).

The results obtained here for the Oregonator should be of use in guiding the design of future experiments on the BZ-AOT system, where several cross-diffusion coefficients have already been measured [4,5] and an Oregonator-based model [7] has been developed. Implementation of this approach will, however, require its extension to models with more than two concentration variables.

**Acknowledgments.** We are grateful to Anne De Wit and Pierre Borckmans for helpful discussions. This work was supported by the National Science Foundation through Grant CHE-0615507. I.R.E. thanks the Radcliffe Institute for Advanced Study for a fellowship.

## Appendix A. Equivalence of the CGLE derivation to Kuramoto's formulation in the case of Hopf instability

Here we consider in detail the method of derivation of the AE in the Hopf case to show that it is equivalent to Kuramoto's procedure [5,9]. Using the eigenvector  $\mathbf{U}$  in the form of (57), the deviations are chosen as

$$\mathbf{X}_1 = \mathbf{U}W e^{i\alpha_0 t} + \bar{\mathbf{U}}\bar{W} e^{-i\alpha_0 t} = \begin{pmatrix} x_{u1} \\ x_{v1} \end{pmatrix} = \begin{pmatrix} \alpha_1 \\ \alpha_2 \end{pmatrix} W e^{i\alpha_0 t} + \begin{pmatrix} \bar{\alpha}_1 \\ \bar{\alpha}_2 \end{pmatrix} \bar{W} e^{-i\alpha_0 t}, \quad (\text{A1})$$

$$\mathbf{X}_2 = \mathbf{V}_0 + \mathbf{V}_2 e^{2i\alpha_0 t} + \bar{\mathbf{V}}_2 e^{-2i\alpha_0 t} = \begin{pmatrix} x_{u2} \\ x_{v2} \end{pmatrix} = \begin{pmatrix} a_0 \\ b_0 \end{pmatrix} + \left[ \begin{pmatrix} a_2 \\ b_2 \end{pmatrix} e^{2i\alpha_0 t} + c.c. \right]. \quad (\text{A2})$$

Here  $W = W(\tau, R)$ ,  $V_{0,2} = V_{0,2}(W, \bar{W})$ . The first harmonics in the second deviation (A2) vanish because there are only the zeroth and second harmonics in  $\mathbf{I}_2$  in Eq. (17) for the Hopf case

$$(\partial / \partial t - \mathbf{J}_0) \mathbf{X}_2 = \mathbf{H}_0 \mathbf{X}_1 \mathbf{X}_1 \equiv \mathbf{I}_2 \quad (\text{A3})$$

with

$$\mathbf{H}_0 \mathbf{X}_1 \mathbf{X}_1 = (\mathbf{H}_0 \mathbf{U} \mathbf{U}) W^2 e^{2i\alpha_0 t} + 2(\mathbf{H}_0 \mathbf{U} \bar{\mathbf{U}}) |W|^2 + (\mathbf{H}_0 \bar{\mathbf{U}} \bar{\mathbf{U}}) \bar{W}^2 e^{-2i\alpha_0 t} \quad (\text{A4})$$

or in the coordinate form

$$\begin{aligned} (\mathbf{H}_0 \mathbf{X}_1 \mathbf{X}_1)_j &= \left[ H_j^{uu} \alpha_1 \bar{\alpha}_1 + H_j^{uv} (\alpha_1 \bar{\alpha}_2 + \alpha_2 \bar{\alpha}_1) + H_j^{vv} \alpha_2 \bar{\alpha}_2 \right] |W|^2 + \\ & \left[ \frac{1}{2} (H_j^{uu} \alpha_1^2 + 2H_j^{uv} \alpha_1 \alpha_2 + H_j^{vv} \alpha_2^2) W^2 e^{2i\alpha_0 t} + c.c. \right] \equiv 2G_j^0 |W|^2 + (G_j^+ W^2 e^{2i\alpha_0 t} + c.c.), \quad j = 1, 2. \end{aligned} \quad (\text{A5})$$

This fact was pointed out by Kuramoto [9,13]. Then, the application of the above procedure for the second order yields for the zeroth harmonic terms the following equations

$$-J_{11}^0 a_0 - J_{12}^0 b_0 = 2G_1^0 |W|^2, \quad (\text{A6})$$

$$-J_{21}^0 a_0 - J_{22}^0 b_0 = 2G_2^0 |W|^2, \quad (\text{A7})$$

from which the coefficients  $a_0, b_0$  are found as in Eqs. (43) and (44) with only one replacement  $G_j \rightarrow G_j^0$ . In vector form we can write these two equations as

$$-\mathbf{J}_0 \mathbf{V}_0 = 2 \begin{pmatrix} G_1^0 \\ G_2^0 \end{pmatrix} |W|^2 = 2(\mathbf{H}_0 \mathbf{U} \bar{\mathbf{U}}) |W|^2. \quad (\text{A8})$$

Hence

$$\mathbf{V}_0 = -2\mathbf{J}_0^{-1} (\mathbf{H}_0 \mathbf{U} \bar{\mathbf{U}}) |W|^2. \quad (\text{A9})$$

The same procedure for the second harmonics yields Eqs. (48) and (49) for  $a_2, b_2$  with the following replacements:  $G_j \rightarrow G_j^+$  and

$$\varphi_{mn} = -J_{mn}^0 + 2i\omega_0 \delta_{mn}, \quad \delta_{mn} = \begin{cases} 1, & m = n, \\ 0, & m \neq n, \end{cases} \quad m, n = 1, 2, \quad (\text{A10})$$

so that the equation for  $a_2, b_2$  can be written in vector form as

$$\varphi \mathbf{V}_2 = -(\mathbf{J}_0 - 2i\omega_0) \mathbf{V}_2 = \begin{pmatrix} G_1^+ \\ G_2^+ \end{pmatrix} W^2 = (\mathbf{H}_0 \mathbf{U} \mathbf{U}) W^2, \quad (\text{A11})$$

i.e.,

$$\mathbf{V}_2 = -(\mathbf{J}_0 - 2i\omega_0)^{-1} (\mathbf{H}_0 \mathbf{U} \mathbf{U}) W^2. \quad (\text{A12})$$

For the third order of expansion with

$$\mathbf{I}_3 = -\frac{\partial \mathbf{X}_1}{\partial \tau} + \mathbf{J}_1 \mathbf{X}_1 + \mathbf{D}_0 \frac{\partial^2 \mathbf{X}_1}{\partial R^2} + 2\mathbf{H}_0 \mathbf{X}_1 \mathbf{X}_2 + \mathbf{N}_0 \mathbf{X}_1 \mathbf{X}_1 \mathbf{X}_1 \quad (\text{A13})$$

the quadratic term

$$(\mathbf{H}_0 \mathbf{X}_1 \mathbf{X}_2)_j = \frac{1}{2} \left[ H_j^{uu} x_{u1} x_{u2} + H_j^{uv} (x_{u1} x_{v2} + x_{v1} x_{u2}) + H_j^{vv} x_{v1} x_{v2} \right] \quad (\text{A14})$$

has contributions proportional to  $e^{i\omega t}$  :

$$\begin{aligned} x_{u1} x_{u2} &= (\alpha_1 W a_0 + \bar{\alpha}_1 \bar{W} a_2) e^{i\omega t} + \dots, & x_{u1} x_{v2} &= (\alpha_1 W b_0 + \bar{\alpha}_1 \bar{W} b_2) e^{i\omega t} + \dots, \\ x_{v1} x_{u2} &= (\alpha_2 W a_0 + \bar{\alpha}_2 \bar{W} a_2) e^{i\omega t} + \dots, & x_{v1} x_{v2} &= (\alpha_2 W b_0 + \bar{\alpha}_2 \bar{W} b_2) e^{i\omega t} + \dots, \end{aligned} \quad (\text{A15})$$

or in vector form

$$\mathbf{H}_0 \mathbf{X}_1 \mathbf{X}_2 = (\mathbf{H}_0 \mathbf{U} \mathbf{V}_0) W e^{i\omega t} + (\mathbf{H}_0 \bar{\mathbf{U}} \mathbf{V}_2) \bar{W} e^{i\omega t} + \dots \quad (\text{A16})$$

The same manipulation with the cubic term

$$(\mathbf{N}_0 \mathbf{X}_1 \mathbf{X}_1 \mathbf{X}_1)_j = \frac{1}{6} \left[ N_j^{uuu} x_{u1}^3 + 3N_j^{uuv} x_{u1}^2 x_{v1} + 3N_j^{uvv} x_{u1} x_{v1}^2 + N_j^{vvv} x_{v1}^3 \right] \quad (\text{A17})$$

results in contributions like

$$x_{u1}^3 = 3\alpha_1^2 \bar{\alpha}_1 |W|^2 W e^{i\omega t} + \dots, \quad (\text{A18})$$

or in vector form

$$\mathbf{N}_0 \mathbf{X}_1 \mathbf{X}_1 \mathbf{X}_1 = 3(\mathbf{N}_0 \mathbf{U} \mathbf{U} \bar{\mathbf{U}}) |W|^2 W e^{i\omega t} + \dots \quad (\text{A19})$$

Taking into account (A9) and (A12) we put  $\mathbf{V}_0 = \tilde{\mathbf{V}}_0 |W|^2$  and  $\mathbf{V}_2 = \mathbf{V}_+ W^2$  and recover

Kuramoto's result [9,13]

$$\mathbf{I}_3^+ = -\frac{\partial \mathbf{U} W}{\partial \tau} + \mathbf{J}_1 \mathbf{U} W + \mathbf{D}_0 \frac{\partial^2 \mathbf{U} W}{\partial R^2} + 2(\mathbf{H}_0 \mathbf{U} \mathbf{V}_0 + \mathbf{H}_0 \bar{\mathbf{U}} \mathbf{V}_+) |W|^2 W + 3(\mathbf{N}_0 \mathbf{U} \mathbf{U} \bar{\mathbf{U}}) |W|^2 W, \quad (\text{A20})$$

where the tilde over  $\mathbf{V}_0$  has been omitted.

## Appendix B. Calculation of the $c_2$ coefficient in the CGLE for the Oregonator model

The calculation follows Kuramoto's approach for deriving the CGLE [9]. To find

$c_2 = g''/g'$  in the CGLE we calculate the vectors  $\mathbf{HXX}$  and  $\mathbf{NXXX}$ . For  $\mathbf{HXX}$ , we have

$$(\mathbf{HXX})_i = \frac{1}{2} \left[ \frac{\partial^2 F_i(u, v)}{\partial u^2} \Big|_{u_0, v_0} U_u U_u + 2 \frac{\partial^2 F_i(u, v)}{\partial u \partial v} \Big|_{u_0, v_0} U_u U_v \right]. \quad (\text{B1})$$

where the two components of eigenvector  $\mathbf{U}$ ,  $U_u$  and  $U_v$ , are used for the deviation  $\mathbf{X}$ .

Here we have taken into account that  $H_1^{vv} = \frac{\partial^2 F_1(u, v)}{\partial v^2} = 0$  for the Oregonator model,

and, since  $F_2(u, v)$  is a linear function, all its second derivatives are zero, which causes

the second component  $(\mathbf{HXX})_2$  of the vector  $\mathbf{HXX}$  to vanish. With  $\mu = 0$  (or  $\varepsilon = \varepsilon_{\text{cH}}$ )

the first component  $(\mathbf{H}_0 \mathbf{XX})_1$  [see Eq. (B1)] is given by

$$(\mathbf{H}_0 \mathbf{XX})_1 = (1 - \omega_0^2) H_1^{uu} / 2 + H_1^{uv} + i\omega_0 (H_1^{uu} + H_1^{uv}), \quad (\text{B2})$$

$$(\mathbf{H}_0 \mathbf{XX})_1 = (1 + \omega_0^2) H_1^{uu} / 2 + H_1^{uv}, \quad (\text{B3})$$

where  $H_1^{uu} = \frac{\partial^2 F_1(u, v)}{\partial u^2} \Big|_{u_0, v_0; \mu=0} = -\frac{2}{\varepsilon_{\text{cH}}} \left[ 1 - \frac{2qfv_0}{(q+u_0)^3} \right],$

$$H_1^{uv} = \frac{\partial^2 F_1(u, v)}{\partial u \partial v} \Big|_{u_0, v_0; \mu=0} = \frac{\partial^2 F_1(u, v)}{\partial v \partial u} \Big|_{u_0, v_0; \mu=0} = -\frac{2}{\varepsilon_{\text{cH}}} \frac{qf}{(q+u_0)^2}, \quad U_u U_u = 1 + 2i\omega_0 - \omega_0^2,$$

$$U_u \overline{U_u} = 1 + \omega_0^2, \quad \overline{U_u} U_v = 1 - i\omega_0, \quad \text{and} \quad U_u U_v = 1 + i\omega_0.$$

Now we calculate the vectors  $\mathbf{NXXX}$  and  $\mathbf{NXXX}$ . The non-zero terms of the first component are

$$(NXXX)_1 = \frac{1}{6} \left[ \frac{\partial^3 F_1(u, v)}{\partial u^3} \Big|_{u_0, v_0} U_u U_u U_u + 3 \frac{\partial^3 F_1(u, v)}{\partial u^2 \partial v} \Big|_{u_0, v_0} U_u U_u U_v \right], \quad (B4)$$

$$(NXXX\bar{X})_1 = \frac{1}{6} \left[ \frac{\partial^3 F_1(u, v)}{\partial u^3} \Big|_{u_0, v_0} U_u U_u \bar{U}_u + \frac{\partial^3 F_1(u, v)}{\partial u^2 \partial v} \Big|_{u_0, v_0} (2U_u U_v \bar{U}_u + U_u U_u \bar{U}_v) \right]. \quad (B5)$$

The second component  $(NXXX)_2 = 0$  for the Oregonator. With  $\mu = 0$  (or  $\varepsilon = \varepsilon_{\text{cH}}$ ) the

first component  $(N_0XXX\bar{X})_1$  reads

$$(N_0XXX\bar{X})_1 = (1/6) \left[ N_1^{uuu} (1 + i\omega_0) (1 + \omega_0^2) + N_1^{uvv} (3 + 2i\omega_0 + \omega_0^2) \right], \quad (B6)$$

where  $N_1^{uuu} = \frac{\partial^3 F_1(u, v)}{\partial u^3} \Big|_{u_0, v_0} = -\frac{1}{\varepsilon_{\text{cH}}} \frac{12qfv_0}{(q+u_0)^4}$ ,  $N_1^{uvv} = \frac{\partial^3 F_1(u, v)}{\partial u^2 \partial v} \Big|_{u_0, v_0} = \frac{1}{\varepsilon_{\text{cH}}} \frac{4qf}{(q+u_0)^3}$ ,

$$U_u U_u \bar{U}_u = (1 + i\omega_0)^2 (1 - i\omega_0), \quad U_u U_v \bar{U}_u = 1 + \omega_0^2, \quad U_u U_u \bar{U}_v = 1 + 2i\omega_0 - \omega_0^2.$$

To complete the calculation of  $c_2$ , we first compute a few intermediate expressions (see Ref. [9]) like  $3(U_u^* N_0 XXX\bar{X})_1$ ,  $\mathbf{J}_0^{-1}$ ,  $(\mathbf{J}_0 - 2i\omega_0)^{-1}$ ,  $\mathbf{V}_0 \equiv -2\mathbf{J}_0^{-1} \mathbf{H}_0 \mathbf{X} \bar{\mathbf{X}}$ , and

$\mathbf{V}_+ \equiv -(\mathbf{J}_0 - 2i\omega_0)^{-1} \mathbf{H}_0 \mathbf{X} \mathbf{X}$ . Next we derive

$$3(U_u^* N_0 XXX\bar{X})_1 = \left[ N_1^{uuu} (1 + \omega_0^2) + 2N_1^{uvv} \right] / 4 - (i/\omega_0) \left[ N_1^{uuu} (1 + \omega_0^2) + N_1^{uvv} (3 + \omega_0^2) \right] / 4, \quad (B7)$$

$$\mathbf{J}_0^{-1} = \frac{1}{\omega_0^2} \begin{pmatrix} -1 & 1 + \omega_0^2 \\ -1 & 1 \end{pmatrix}, \quad (B8)$$

$$(\mathbf{J}_0 - 2i\omega_0)^{-1} = -\frac{1}{3\omega_0^2} \begin{pmatrix} -1 - 2i\omega_0 & 1 + \omega_0^2 \\ -1 & 1 - 2i\omega_0 \end{pmatrix}, \quad (B9)$$

$$\mathbf{V}_0 = -2\mathbf{J}_0^{-1} \mathbf{H}_0 \mathbf{X} \bar{\mathbf{X}} = \begin{pmatrix} \frac{1 + \omega_0^2}{\omega_0^2} H_1^{uu} + \frac{2}{\omega_0^2} H_1^{uv} \\ 1 \end{pmatrix} \begin{pmatrix} 1 \\ 1 \end{pmatrix}, \quad (B10)$$

$$\mathbf{V}_+ = -(\mathbf{J}_0 - 2i\omega_0)^{-1} \mathbf{H}_0 \mathbf{X} \mathbf{X} = -\frac{1}{3\omega_0^2} \left[ \frac{1 - \omega_0^2}{2} H_1^{uu} + H_1^{uv} + i\omega_0 (H_1^{uu} + H_1^{uv}) \right] \begin{pmatrix} 1 + 2i\omega_0 \\ 1 \end{pmatrix}, \quad (B11)$$

$$(\mathbf{H}_0 \mathbf{U} \mathbf{V}_0)_1 = [H_1^{uu} U_u V_{0u} + H_1^{uv} (U_u V_{0v} + U_v V_{0u})] / 2 \quad (\text{B12})$$

and  $(\mathbf{H}_0 \mathbf{U} \mathbf{V}_0)_2 = 0$ , where  $V_{0u}$  and  $V_{0v}$  are the first and the second components of  $\mathbf{V}_0$ , respectively.

Next, we determine (following Kuramoto [9]) the complex function  $g$  as

$$g \equiv g' + ig'' = -\mathbf{U}^* \cdot (2\mathbf{H}_0 \mathbf{U} \mathbf{V}_0 + 2\mathbf{H}_0 \bar{\mathbf{U}} \mathbf{V}_+ + 3N_0 \mathbf{X} \bar{\mathbf{X}}). \quad (\text{B13})$$

The first term of the r.h.s. of (B13) gives

$$-2\mathbf{U}^* \mathbf{H}_0 \mathbf{U} \mathbf{V}_0 = \frac{1}{2} \left( \frac{1 + \omega_0^2}{\omega_0^2} H_1^{uu} + \frac{2}{\omega_0^2} H_1^{uv} \right) \left[ -(H_1^{uu} + H_1^{uv}) + \frac{i}{\omega_0} (H_1^{uu} + 2H_1^{uv}) \right]. \quad (\text{B14})$$

The second term of the r.h.s. of (B13), defined by

$$(\mathbf{H}_0 \bar{\mathbf{U}} \mathbf{V}_+)_1 = \left[ H_1^{uu} \bar{U}_u V_{+u} + H_1^{uv} (\bar{U}_u V_{+v} + \bar{U}_v V_{+u}) \right] / 2 \quad \text{and} \quad (\mathbf{H}_0 \bar{\mathbf{U}} \mathbf{V}_+)_2 = 0, \quad \text{reads}$$

$$\begin{aligned} -2\mathbf{U}^* \mathbf{H}_0 \bar{\mathbf{U}} \mathbf{V}_+ &= \frac{1}{2\omega_0^2} (H_1^{uu} + H_1^{uv}) \left( \frac{1 + \omega_0^2}{2} H_1^{uu} + H_1^{uv} \right) - \\ &\frac{i}{6\omega_0^3} \left[ \left( \frac{1 - \omega_0^2}{2} H_1^{uu} + H_1^{uv} \right) \left[ (1 + 2\omega_0^2) H_1^{uu} + 2H_1^{uv} \right] - \omega_0^2 (H_1^{uu} + H_1^{uv})^2 \right]. \end{aligned} \quad (\text{B15})$$

The last term in this expression is given by (B7). Collecting all terms, we obtain the following expressions for  $g'$  and  $g''$ :

$$g' = -\frac{1}{2\omega_0^2} (H_1^{uu} + H_1^{uv}) \left( \frac{1 + \omega_0^2}{2} H_1^{uu} + H_1^{uv} \right) - \frac{1}{2} \left( \frac{1 + \omega_0^2}{2} N_1^{uuu} + N_1^{uuv} \right), \quad (\text{B16})$$

$$g'' = -\frac{g'}{\omega_0} + \frac{1}{6\omega_0^3} \left[ 2(1 + \omega_0^2) H_1^{uu} + 7H_1^{uv} \right] \left( \frac{1 + \omega_0^2}{2} H_1^{uu} + H_1^{uv} \right)^2 + \frac{1}{6\omega_0} (H_1^{uv})^2 + \frac{1}{2\omega_0} \frac{1 + \omega_0^2}{2} N_1^{uuv}. \quad (\text{B17})$$

## References

- [1] V. K. Vanag and I. R. Epstein, *Phys. Chem. Chem. Phys.* **11**, 897 (2009).
- [2] M. Cross and H. Greenside, *Pattern Formation and Dynamics in Nonequilibrium Systems* (Cambridge University Press, Cambridge, 2009).
- [3] A. M. Turing, *Philos. Trans. R. Soc. London. Ser. B* **237**, 37 (1952).
- [4] F. Rossi, V. K. Vanag, E. Tiezzi, and I. R. Epstein, *J. Phys. Chem. B* **114**, 8140 (2010).
- [5] F. Rossi, V. K. Vanag, and I. R. Epstein, *Chem. Eur. J.* **17**, 2138 (2011).
- [6] V. K. Vanag, F. Rossi, A. A. Cherkashin, and I. R. Epstein, *J. Phys. Chem. B* **112**, 9058 (2008).
- [7] V. K. Vanag and I. R. Epstein, *Phys. Rev. Lett.* **87**, 228301 (2001).
- [8] M. C. Cross and P. C. Hohenberg, *Rev. Mod. Phys.* **65**, 851 (1993).
- [9] Y. Kuramoto, *Chemical Oscillations, Waves, and Turbulence* (Springer, Berlin, 1984).
- [10] A. C. Newell, in *Lectures in Applied Mathematics. Vol. 15. Nonlinear Wave Motion.*, Edited by A. C. Newell (American Mathematical Society, New York, 1974), Vol. 15, p. 157.
- [11] I. S. Aranson and L. Kramer, *Rev. Mod. Phys.* **74**, 99 (2002).
- [12] D. Walgraef, *Spatiotemporal Pattern Formation* (Springer-Verlag, 1997).
- [13] Y. Kuramoto and T. Tsuzuki, *Prog. Theor. Phys.* **54**, 687 (1975).
- [14] A. De Wit, Thesis, Universite Libre de Bruxelles, 1993.
- [15] M. Ipsen, L. Kramer, and P. G. Sorensen, *Phys. Rep.* **337**, 193 (2000).
- [16] E. M. Nicola, L. Bruschi, and M. Bar, *J. Phys. Chem. B* **108**, 14733 (2004).

- [17] Y. Gong and D. J. Christini, Phys. Rev. Lett. **90**, 088302 (2003).
- [18] C. M. Topaz and A. J. Catlla, Phys. Rev. E **81**, 026213 (2010).
- [19] H. Levine and X. Q. Zou, Phys. Rev. E **48**, 50 (1993).
- [20] R. J. Field and R. M. Noyes, J. Chem. Phys. **60**, 1877 (1974).
- [21] J. J. Tyson and P. C. Fife, J. Chem. Phys. **73**, 2224 (1980).
- [22] G. Nicolis and I. Prigogine, *Self-Organization in Nonequilibrium Systems* (Wiley-Interscience, New York, 1977).
- [23] B. P. Belousov, in *Collection of Short Papers on Radiation Medicine*, (Medgiz, Moscow, 1959), p. 145.
- [24] A. M. Zhabotinsky, Biofizika **9**, 306 (1964).
- [25] M. Ipsen, F. Hynne, and P. G. Sorensen, Int. J. Bifurcation and Chaos **7**, 1539 (1997).
- [26] M. Ipsen, F. Hynne, and P. G. Sorensen, Physica D **136**, 66 (2000).
- [27] D. G. Miller, V. Vitagliano, and R. Sartorio, J. Phys. Chem. **90**, 1509 (1986).
- [28] A. C. Newell and J. A. Whitehead, J. Fluid Mech. **38**, 279 (1969).
- [29] L. A. Segel, J. Fluid Mech. **38**, 203 (1969).
- [30] E. A. Kuznetsov, A. A. Nepomnyashchy, and L. M. Pismen, Phys. Lett. A **205**, 261 (1995).
- [31] G. H. Gunaratne, Q. Ouyang, and H. L. Swinney, Phys. Rev. E **50**, 2802 (1994).
- [32] B. Pena and C. Perez-Garcia, Phys. Rev. E **64**, 056213 (2001).
- [33] R. B. Hoyle, *Pattern Formation. An Introduction to Methods* (Cambridge University Press, Cambridge, 2006).

- [34] R. Courant and D. Hilbert, *Methods of Mathematical Physics* (John Wiley & Sons, New York, 1953), Vol. 1.
- [35] V. K. Vanag and I. R. Epstein, *Science* **294**, 835 (2001).
- [36] V. K. Vanag and I. R. Epstein, *Phys. Rev. Lett.* **88**, 088303 (2002).
- [37] L. Bruschi, E. M. Nicola, and M. Bär, *Phys. Rev. Lett.* **92**, 089801 (2004).
- [38] J. J. Tyson, *J. Chem. Phys.* **62**, 1010 (1975).
- [39] V. K. Vanag and I. R. Epstein, *Phys. Rev. Lett.* **92**, 128301 (2004).

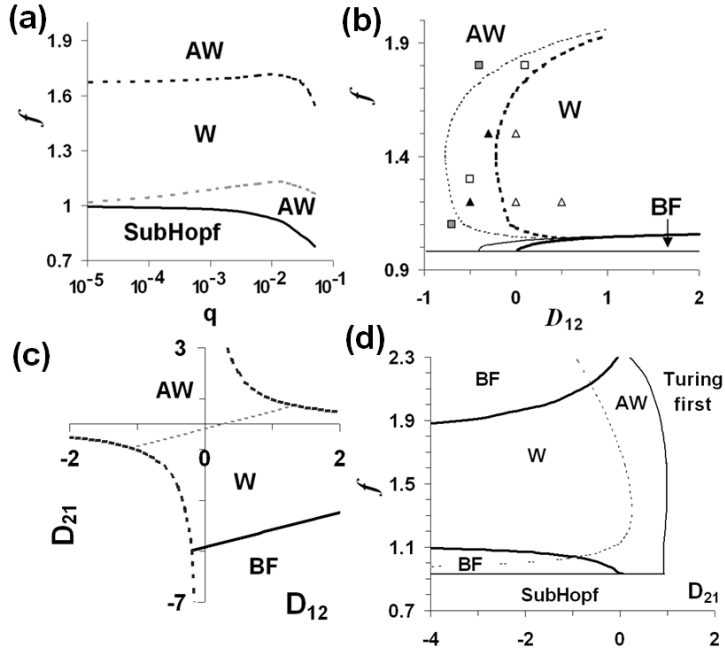


**Fig. 1.** Parameter planes for the Oregonator model. (a) Dependence of  $f_c$  (bold line) and  $f_{AW}$  (two dashed lines) on  $q$ . Dashed lines ( $f_{AW}$ ) mark the boundary between normal wave (W) and antiwave (AW) domains at  $D_{11} = 1$ , and  $D_{12} = D_{21} = 0$ . (b) Domains of Benjamin-Feir (BF) instability, waves, and antiwaves in the  $D_{12} - f$  plane at  $q = 0.001$ ,  $D_{21} = 0$ ,  $D_{11} = 1$  (bold lines), 1.5 (thinner lines). At larger  $D_{11}$  all curves (dashed and bold) shift to the left. The leftmost point of the boundary between the AW and W domains is at  $D_{12} \cong -0.22$  for  $D_{11} = 1$  and at  $D_{12} = -0.8$  for  $D_{11} = 1.5$ , while the BF domain ends at  $D_{12} \cong 0.01$  for  $D_{11} = 1$  and at  $D_{12} = -0.5$  for  $D_{11} = 1.5$ . (c) Domains of BF, W, and AW in the  $D_{12}$ - $D_{21}$  plane at  $f = 1.1$ ,  $q = 0.01$ ,  $D_{11} = 1$ ,  $c_2 = 0.1917$ , hyperbolic curves correspond to the condition  $\det \mathbf{D} = 0$ ; (d) Domains of BF, W, and AW in the  $D_{21}$ - $f$  plane at  $q = 0.01$ ,  $D_{12} = 0$ ,  $D_{11} = 1$ . Numerical integration of Eqs. (30),(31) was performed at the marked points in Fig. 1b. Triangles correspond to  $D_{11} = 1$ , squares to  $D_{11} = 1.5$ ; black symbols show antiwaves, white symbols waves.  $D_{22} = 1$  for all cases.

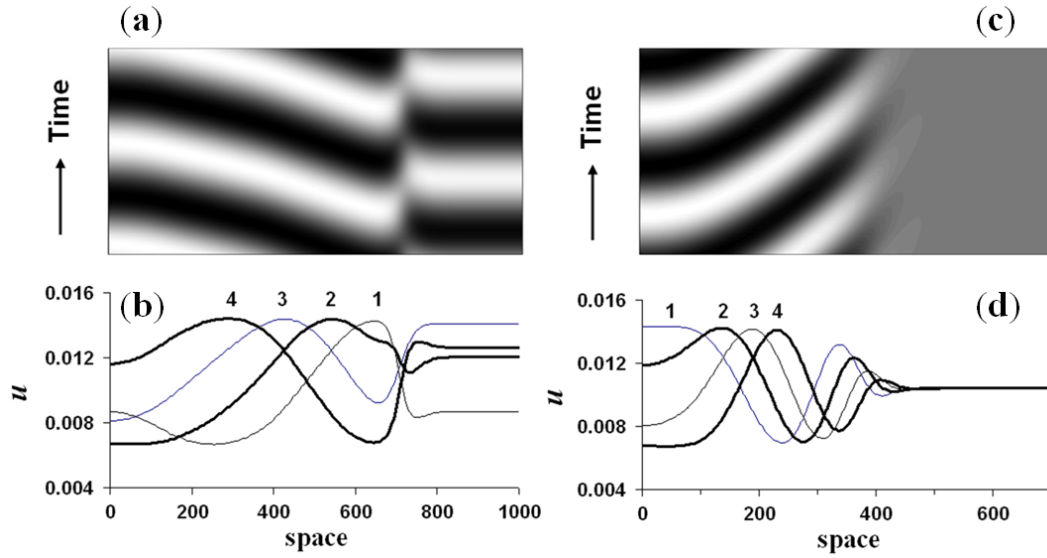


**Fig. 2.** Examples of antiwaves (left column) and waves (right column) in 1D Oregonator model induced by cross-diffusion coefficient  $D_{12}$ . Parameters:  $f = 1.2$ ,  $q = 10^{-3}$ ,  $\varepsilon = 0.78$  ( $\varepsilon_{\text{cH}} = 0.78723$ ),  $D_{11} = D_{22} = 1$ ,  $D_{21} = 0$ ,  $D_{12} =$  (left column)  $-0.5$ , (right column)  $1$ ,  $c_1 + c_2 =$  (left column)  $0.33745$ , (right column)  $-1.1418$ ;  $c_1 - c_2 =$  (left column)  $0.64872$ , (right column)  $-0.83053$ . Total time for both space-time plots is equal to 25. Numbers 1 – 4 for the profiles of the variable  $u$  correspond to relative times 5, 7, 9, and 11, respectively (starting from an arbitrary time long after the initial perturbation). Zero-flux boundary conditions.

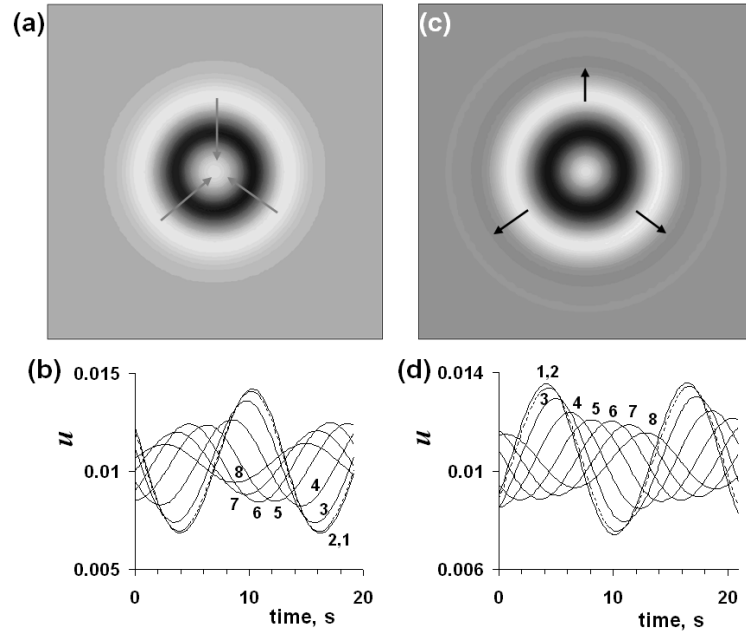


**Fig. 3.** Examples of circular antiwaves (left column) and waves (right column) in 2D Oregonator model induced by cross-diffusion coefficient  $D_{12}$ . Parameters as in Fig. 2:  $f = 1.2$ ,  $q = 10^{-3}$ ,  $\varepsilon = 0.78$ ,  $D_{11} = D_{22} = 1$ ,  $D_{21} = 0$ ,  $D_{12} =$  (left column)  $-0.5$ , (right column)  $1$ . Size of (a) and (c) is  $900 \times 900$ . White color corresponds to the minimum of activator  $u$  and black to the maximum. Numbers 1 – 8 in (b) and (d) correspond to the spatial points at the distances  $0, R/16, 2R/16, 3R/16, 4R/16, 5R/16, 6R/16, 7R/16$  from the center, respectively (starting from an arbitrary time long after the initial perturbation made in the center). Zero-flux boundary conditions.

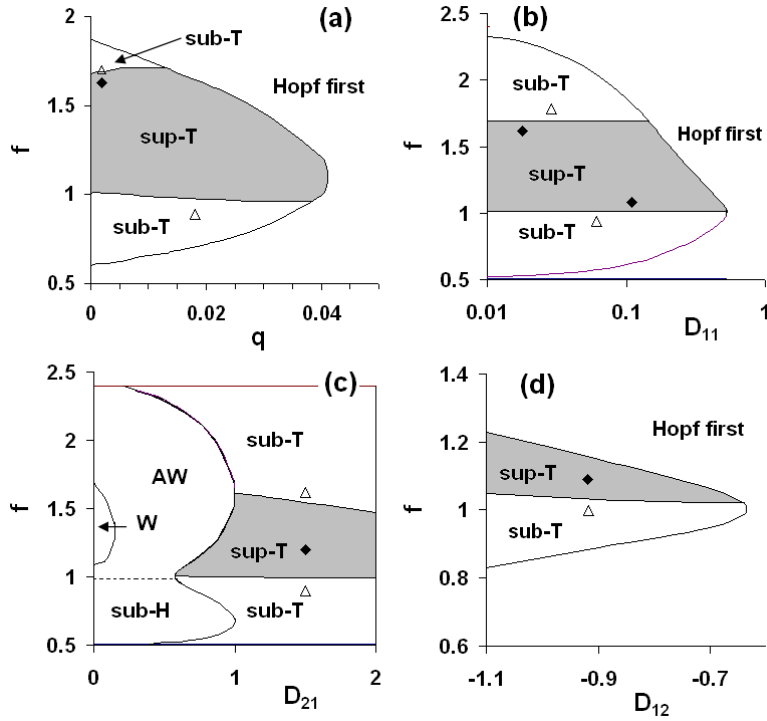


**Fig. 4.** Parameter planes for the Oregonator model showing regions of super- and subcritical Turing instability obtained by determining the sign of  $g$  in Eq. (4). Black rhombs and white triangles correspond to super- and sub-critical Turing patterns, respectively, obtained in numerical simulations. In panel (c), regions in which Hopf bifurcation occurs first are subdivided into regions with super- and subcritical Hopf bifurcation, and the supercritical Hopf region is further divided into regions of waves (W) and anti-waves (AW) on the basis of the CGLE. Parameters:  $D_{22} = 1$ ,  $D_{11} =$  (a) 0.1, (c, d) 1,  $D_{12} =$  (a - c) 0,  $D_{21} =$  (a, b, d) 0,  $q =$  (b - d) 0.001;  $\varepsilon = \varepsilon_{cH}$  [see Eq. (60)] for the region in which Hopf bifurcation starts first,  $\varepsilon = \varepsilon_{cT}$  [see Eq. (62)] for the region in which Turing bifurcation starts first. TAE is valid only in areas shaded in gray.

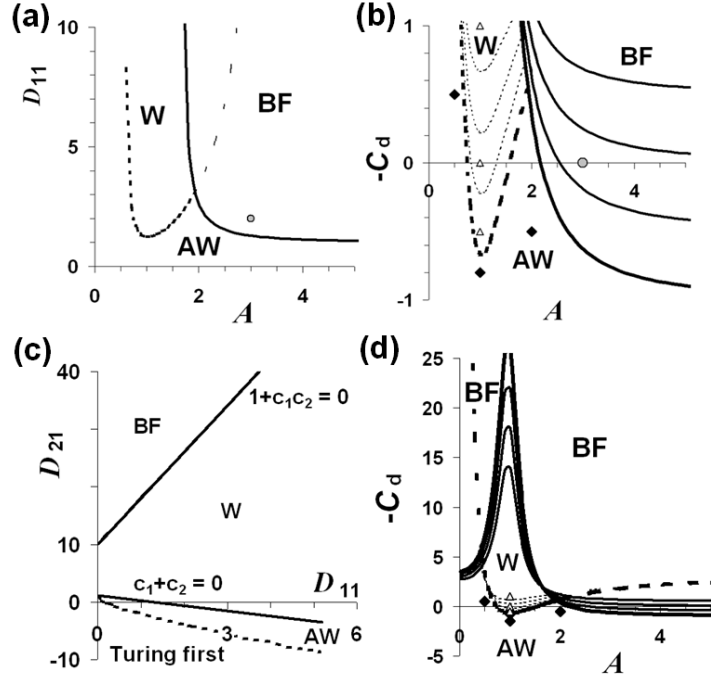


**Fig. 5.** Domains of Benjamin-Feir (BF) instability, waves (W), and antiwaves (AW) for Brusselator model in (a) the  $A-D_{11}$  plane at  $D_{12} = D_{21} = 0$  and (b) the  $A-D_{21}$  plane at  $D_{12} = 0$  [ $-C_d = D_{21} - D_{12}(1 + 1/\omega_0^2)$ ]. In (b), dotted (boundary between wave and antiwave domains) and bold (boundary between regular and chaotic (BF) waves) curves from top to bottom are obtained at  $D_{11} = 0.5, 1, 1.5,$  and  $2$ . The BF instability develops in the area above the bold curves. Plot (d) is an enlargement of plot (b). (c) Three domains (BF, W, and AW) in the  $D_{11} - D_{21}$  plane at  $A = 1$  and  $D_{12} = 0$ . W-domain in (a) is limited by two vertical lines corresponding to two roots of the equation  $A^4 - 13A^2 + 4 = 0$  ( $A_{\text{left}} \approx 0.56$  and  $A_{\text{right}} \approx 3.56$ ). BF domain in (a) exists only at  $A > \sqrt{5 + \sqrt{33}} / 2 \approx 1.64$  (a root of equation  $2A^4 - 5A^2 - 1 = 0$ ). Symbols mark points at which the model was numerically integrated at  $D_{11} = 2$  (gray dot, BF instability; white triangle, waves; black rhombs for antiwaves).  $D_{22} = 1$  for all panels.

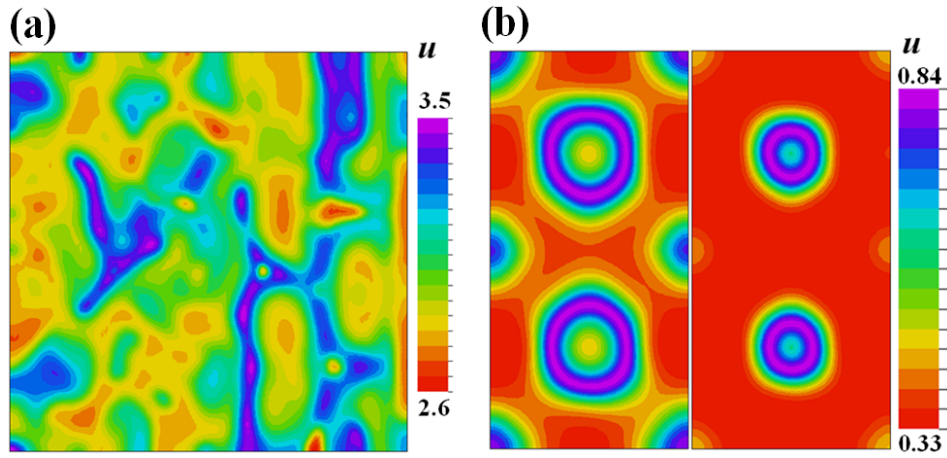


**Fig. 6.** Patterns in the Brusselator model. (a) Example of BF turbulence at  $A = 3$ ,  $B = 10.05$ ,  $D_{11} = 2$ ,  $D_{22} = 1$ , and  $D_{12} = D_{21} = 0$ ,  $1 + c_1c_2 = -1.6767$ ; size =  $450 \times 450$ . (b) Example of AW at  $A = 0.5$ ,  $B = 1.35$ ,  $D_{11} = 2$ ,  $D_{22} = 1$ ,  $D_{12} = 0$ , and  $D_{21} = 0.5$ ,  $c_1 + c_2 = 0.490741$  ( $c_1 - c_2 = -0.99074$ ). Two snapshots (with dimensions  $450 \times 900$ ) in (b) are separated in time by  $\Delta t = 2$  (the two circular waves in the middle shrink). Zero-flux boundary conditions.

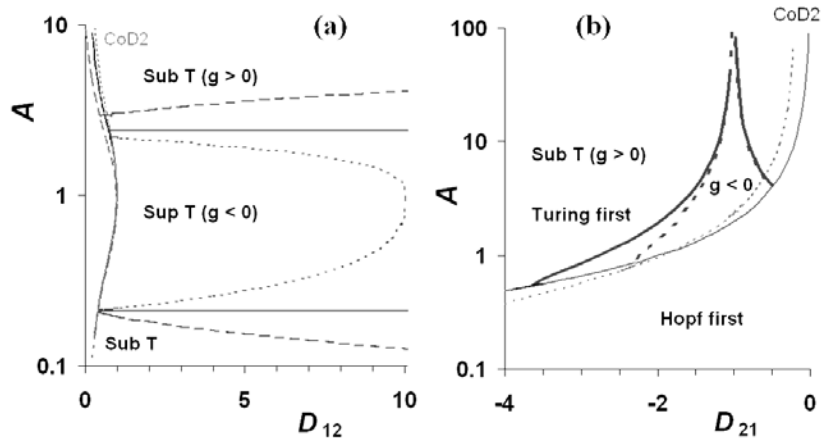


**Fig. 7.** Areas of super- ( $g < 0$ ) and subcritical ( $g > 0$ ) Turing instability in the Brusselator model. Parameters:  $D_{11} = D_{22} = 1$ . Bold lines in (a) and (b):  $D_{21} = 0$  and  $D_{12} = 0$ , respectively. Dotted lines in (a) (with closed loop):  $D_{21} = 0.1$ ; dashed line in (a):  $D_{21} = -0.2$ . Dashed lines in (b):  $D_{12} = -0.2$ . CoD2 signifies a codimension two bifurcation, where Turing and Hopf instabilities start simultaneously.